Stem Cell Research & Therapy

RESEARCH

Open Access

Deep-freezing and decontamination strategy for a large autologous bone graft with presentation of the osteogenic potential of resident osteoblasts

Marija Zekušić[1,2*†], Marija Skoko[1,3†], Kruno Vukušić[4], Maja Ledinski[1], Marina Bujić Mihica[1], Dejan Blažević[3,5,6], Zlata A. Sošić[7], Mario Đura[4], Jelena Martinčić[4], Ivana Vrgoč Zimić[1], Ivanka Batarilo[8], Denis Polančec[9], Lucija Zenić[9], Snježana Ramić[10], Patricija Sesar[10], Kristina Crkvenac Gornik[11,12], Slaven Babić[3,5], Jure Pavešić[5], Srećko Sabalić[5,13], Iva M. Tolić[4], Inga Urlić[14], Stanka Misir Šitum[3,15], Tiha Vučemilo[1,3] and Dinko Vidović[5,12,16]

Abstract

Background Musculoskeletal injuries resulting from high-impact trauma often lead to extensive bone defects that require effective reconstruction to prevent limb amputation. However, contamination of large autologous bone grafts in open fractures remains a major clinical challenge. This study aimed to establish a reliable protocol for decontamination of massive autologous bone graft and to assess the viability and regenerative potential of osteoblasts from frozen bone, including the effects of deep freezing and the cryoprotectant dimethyl sulfoxide (DMSO).

Methods A 28 cm femoral segment, extruded during a high-energy road traffic accident, was stored at − 80 °C for 15 days before microbiological analysis revealed contamination. The bone was thawed, decontaminated, and successfully reimplanted. To validate this protocol, femoral head fragments were experimentally contaminated with various microbial strains and treated using the same procedure. To evaluate how low-temperature storage (15 and 30 days, with or without DMSO) impacts osteoblasts, cells were isolated from both fresh and frozen bone and analyzed using a panel of cellular and molecular biology techniques, including histology, flow cytometry, immunofluorescence, gene expression analysis, and real-time imaging.

Results The decontamination protocol effectively eliminated microbial contamination from both the clinical autograft and experimentally treated femoral head fragments, with minimal antibiotic residues. Histological analysis confirmed preservation of osteoblasts, osteocytes, and chondrocytes in frozen bone. Osteoblasts from frozen bone retained proliferative and differentiation capacities comparable to those from fresh bone, with no evidence of mitotic

†Marija Zekušić and Marija Skoko have contributed equally to this work.

*Correspondence:
Marija Zekušić
marija.zekusic@kbcsm.hr

Full list of author information is available at the end of the article

chromosomal instability. Cryopreservation with DMSO-containing media slightly increased population doubling time. Expression of RUNX2 was highest in fresh and 15-day frozen bone, while reduced in 30-day samples. No significant differences were observed between DMSO and non-DMSO groups regarding osteogenic potential. *ALPL* and *COL1A1* expression significantly increased after 14 days of osteogenic induction. Time-lapse imaging demonstrated active osteoblast migration and division, and the presence of extracellular vesicles and nanotubes indicated functional cellular communication.

Conclusions This proof-of-concept study demonstrates that large autologous bone grafts can be frozen and subsequently decontaminated while retaining viable osteoblasts with high proliferative and regenerative potential. By combining a unique and successful clinical case with controlled experimental analyses, the study offers translational relevance, and the findings on osteoblast viability after freezing are promising.

Keywords Decontamination, Autologous bone, Femoral heads, Analysis of antibiotic residues

Graphical abstract

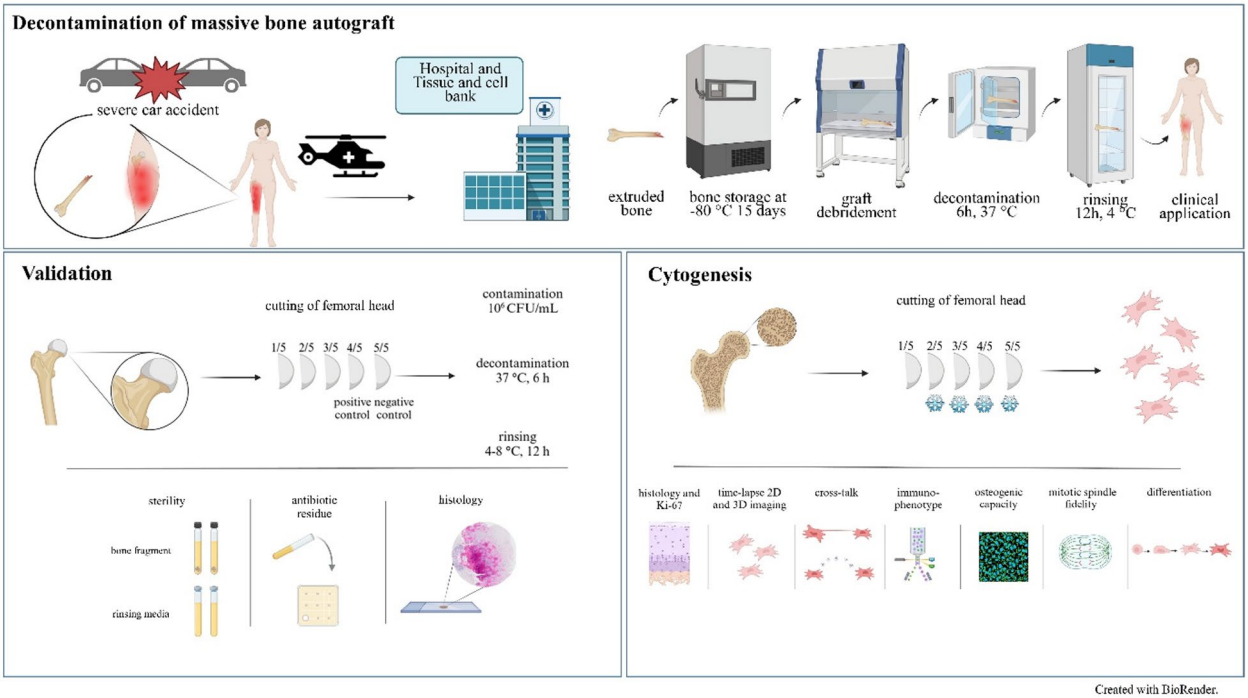

Background

Musculoskeletal injuries, particularly those caused by road traffic accidents and other high-impact events, are among the most common types of trauma and are recognized as a major global health concern [1]. After blood transfusion, human bones, along with other tissues such as tendons, ligaments, skin, heart valves, blood vessels, and corneas, are among the most frequently transplanted tissues [2]. Despite substantial advancements in tissue banking and the increased use of allogeneic bone and synthetic substitutes, autologous bone remains the gold standard in reconstructive bone surgery due to its osteogenic, osteoinductive, osteoconductive, and non-immunogenic properties [3, 4].

In severe trauma cases—such as high-impact traffic accidents involving critical bone loss (e.g., extrusion of a femoral segment)—a key clinical question arises: how can a large, contaminated bone graft be preserved and reused? In life-threatening injuries involving extensive soft tissue and neurovascular damage, amputation is often considered [5]. The decision to amputate or attempt limb salvage is complex, and typically involves a multidisciplinary team including surgeons, cell biologists, and other regenerative medicine experts [6, 7]. Bone loss following transplantation is reported in 11.4% of all open fractures, with the tibia most frequently affected (68%), followed by the femur (22%), primarily in Gustilo type IIIB and IIIC injuries [8, 9, 10], . As such, improving the outcomes of autologous bone transplantation remains a critical objective.

Conventional bone grafting techniques are generally effective for reconstructing defects up to 25 cm in length

in adults, provided a sufficient vascular bed is available [11]. These techniques are commonly applied in lower extremity reconstruction following open fractures, tumor resection, or in osteomyelitis and non-union cases [12]. While allografts from bone banks are an alternative, they are associated with immune responses [11], and unpredictable revision outcomes [13]. The subchondral bone contains bone marrow, blood cells, lipids, and immunogenic proteins [14] which can complicate transplantation. Although fresh frozen allografts, particularly in the proximal femur, have yielded positive results [15], studies show that complete graft osteointegration is rarely achieved [16, 17, 18], . Compared to autologous grafts, allograft integration is slower and less complete [19] making the healing of large defects—especially those caused by trauma or cancer—an ongoing challenge.

The regeneration of large, irregularly shaped autologous osteochondral grafts remains one of the most difficult tasks in orthopedic surgery [20, 21, 22, 23], . When reimplantation of a large autologous femoral segment (including cartilage and ligaments) is considered after high-impact trauma, proper decontamination, rinsing, and storage are essential. This process relies heavily on the expertise of tissue bank specialists. Open fractures are frequently complicated by skeletal infections. Gram-positive bacteria are present in 75% of cases, and Gram-negative bacteria in 25%, posing a serious risk to the patient [24]. Identifying risk factors and implementing effective preventive measures is crucial [25, 26]. A retrospective analysis of 10 035 musculoskeletal tissues found a contamination rate of 52%, with coagulase-negative staphylococci, *Streptococcus* spp., *Bacillus* spp., *Clostridium* spp., and *Staphylococcus aureus* being the most common pathogens [27]. Reported contamination rates for allogenic bone grafts vary widely from 2.5% to 92% [28, 29]. Despite many proposed treatment approaches, no standardized guidelines exist for decontamination or infection prevention during autologous transplantation [5,27].

A further challenge arises when osteochondral grafts require deep freezing. Due to bone's low water content—comprising roughly 10% in young individuals and decreasing to ~ 5% with age [30] the risk of ice crystal formation during freezing is significant. Bone tissue consists of 60% mineral (hydroxyapatite), 30% organic matrix, and only a small proportion of water, which together contribute to its strength and flexibility [31]. While fresh frozen allografts are generally considered non-viable in terms of osteogenic cells [32, 33] some studies report viable cells persisting for months post-freezing [34, 35]. In allogeneic settings, viable cells may trigger immune responses, but in autologous transplantation, they may enhance graft integration and healing.

Bone regeneration depends on four main cell types: osteogenic progenitors, osteoblasts, osteocytes, and osteoclasts. Osteoprogenitor cells, derived from mesenchymal stem cells (MSCs) in the bone marrow, give rise to osteoblasts and osteocytes [36, 37]. Osteoblasts secrete bone matrix and mineralize it via alkaline phosphatase–rich vesicles, while osteoclasts perform bone resorption. Over time, osteoblasts mature into osteocytes, which account for more than 90% of all bone cells [13]. However, it remains unclear whether osteoprogenitor and osteoblast cells retain their functionality after long-term freezing of large bone grafts. Understanding the osteogenic capacity and safety of these cells post-freezing is essential for improving transplantation outcomes.

In this proof-of-concept study, we present, to our knowledge, the first successful decontamination and reimplantation of a large autologous femoral bone segment (28 cm in length) that had been extruded from the body during a high-impact traffic accident. The patient's complete recovery following reimplantation inspired clinicians, molecular biologists and biotechnologists to further explore the viability, potency, and osteogenic potential of cells isolated from deep-frozen bone fragments - challenging the long-standing assumption that cryopreserved bone is biologically inert due to cellular degradation. We therefore hypothesize that, despite cryopreservation, deep-frozen bone may retain osteogenic properties capable of supporting bone regeneration.

Materials and methods

Study design

This proof-of-concept study was designed to evaluate the safety and regenerative potential of massive osteochondral grafts (distal part of femur with ligaments) subjected to contamination, decontamination, freezing, and storage prior to clinical application (illustrated in graphic abstract). The workflow consisted of three main components: Decontamination of massive bone autograft: An extruded osteochondral graft (28 cm), obtained from a patient after a severe traffic accident, was transferred to the Tissue and Cell Bank. The graft was stored at – 80 °C for up to 15 days, followed by debridement, decontamination (37 °C, 6 h), and rinsing (4–8 °C, 12 h) before being released for clinical use. Validation: Experimental validation was conducted under controlled conditions to accurately reproduce and confirm the decontamination and rinsing protocol. Femoral heads were sectioned into segments and experimentally contaminated (10^6 CFU/mL). Samples were subjected to the same decontamination and rinsing protocol, with positive and negative controls included. Sterility, antibiotic residues, and histological analyses were performed on bone fragments and rinsing media to ensure microbiological safety and absence of cytotoxic residues. Cytogenesis: To demonstrate

osteoblast viability after deep-freezing, cells were isolated from bone fragments and characterized using multiple assays. Histology and Ki67 staining were performed to assess proliferation. Additional analyses included 2D and 3D live imaging in division, as well as in single-cell tracking and proliferation dynamics of osteoblasts, cellular cross-talk, immunophenotyping, osteogenic differentiation assays, and evaluation of mitotic spindle fidelity. These analyses provided comprehensive insights into the viability, motility, phenotype and differentiation potential of osteoblasts derived from both fresh and frozen bone.

Decontamination of massive bone autograft (femur)

On August 30, 2019, at approximately 9:00 AM, the patient, M.D. (24 years old), was involved in a road traffic accident. She sustained severe injuries to her right leg, including the following diagnoses: *Severe segmental fracture of the right femur (Gustilo IIIB), open dislocation of the right knee, complex fracture of the right lower leg (Gustilo IIB), lacerated-contused wound of the left thigh, hemorrhagic shock, and traumatic brain concussion.* Initial treatment was provided at the General Hospital Zadar, Croatia. During preliminary examination paramedics brought on emergency department an extruded distal femur wrapped in the plastic bag. After preliminary resuscitation and debridement, bridging with external fixation was done and patient along with extruded femur was transported by helicopter to the Department of Traumatology at Sestre milosrdnice University Hospital Center in Zagreb, Croatia, where she arrived at approximately 4:00 PM. The femur bone, measuring in length, was placed in a separate plastic container partially submerged in a physiological solution used as a transport medium. Upon receipt of the femur bone in the operating room of the Department of Traumatology, a bone swab and a 10 mL sample of the transport medium were collected, and the femur bone was then packaged in a triple sterile plastic bag. Biological samples were sent to the Department of Microbiology at the Croatian Institute for Transfusion Medicine for microbiological analysis, with the aim of detecting the presence of aerobic and anaerobic bacteria, as well as yeast and molds. To obtain more reliable microbiological results, both swabbing and analysis of the transport medium (physiological saline solution) were combined, followed by a 14-day incubation period. The femur bone was subsequently transported to the Tissue and Cell Bank, where it was labeled with the patient's name, date and time of receipt, as well as the bone size, before being stored at -80 °C.

The day before the scheduled surgical procedure for the clinical application of the graft, a process of cleaning, decontamination, and rinsing was carried out at the Tissue Engineering Laboratory of the Tissue and Cell Bank in a microbiological safety cabinet class II (Klimaoprema, Croatia), following a detailed activity plan. First, the graft was cleaned of impurities (glass, plastic, and asphalt) and excess connective tissue, with an initial rinse in physiological solution (Fig. 1). Next, decontamination was performed using 4 L of BASE 128 medium, during which the graft was stored in an incubator at 37 °C for 6 h. After decontamination, the graft was rinsed with 4 L of BASE medium and subsequently stored in a refrigerator at 4–8 °C overnight.

Operation procedure during clinical application of decontaminated femoral graft

A free vascularized fibular graft was used to revascularize the extruded femur. The decontaminated femoral segment measured 28 cm, and the fibular graft measured 21 cm (Fig. 2A). The distal femur was packed with autologous cancellous bone to ensure direct contact between the fibular graft and the femoral condyles. The graft was impacted into the medullary canal and fixed proximally with a single unicortical screw (Fig. 2B). An anterolateral approach was used, respecting the pre-existing stellate scar around the knee. The sciatic nerve and popliteal vessels were identified and protected. The femur–fibular graft composite was inserted and temporarily stabilized with Kirschner wires. Rotational alignment was verified by patellofemoral congruency and the cable technique. Microvascular anastomoses were performed between the fibular graft and the popliteal vessels. Definitive fixation was achieved using a periprosthetic plate (NCB Periprosthetic Plate System, Zimmer–Biomet), allowing stable fixation while preserving the graft's vascular supply (Fig. 2C). The patella was stabilized with a basket plate, and the tibial shaft was bridged using a minimally invasive 3.5 LCP plate. As the femoral condyles were devascularized, ligament healing within the bone tunnels was not expected. The posterior cruciate ligament stump was sutured, and the medial collateral ligament was repaired with anchors at its preserved tibial insertion. The posterolateral corner was partially reconstructed and augmented with an iliotibial band flap anchored near the anterolateral ligament attachment. Postoperatively, the knee was protected in a brace for six weeks, and progressive partial weight bearing was initiated on the first postoperative day.

Validation

Donor assessment

The study was conducted at the Tissue and Cell Bank of the Sestre milosrdnice University Hospital Centre (Zagreb, Croatia), which is authorized by the Ministry of Health of the Republic of Croatia for the collection, processing, and storage of allogeneic (femoral heads) and autologous/cancellous bone in accordance with national legislation. The protocol entitled "Harvesting, Processing,

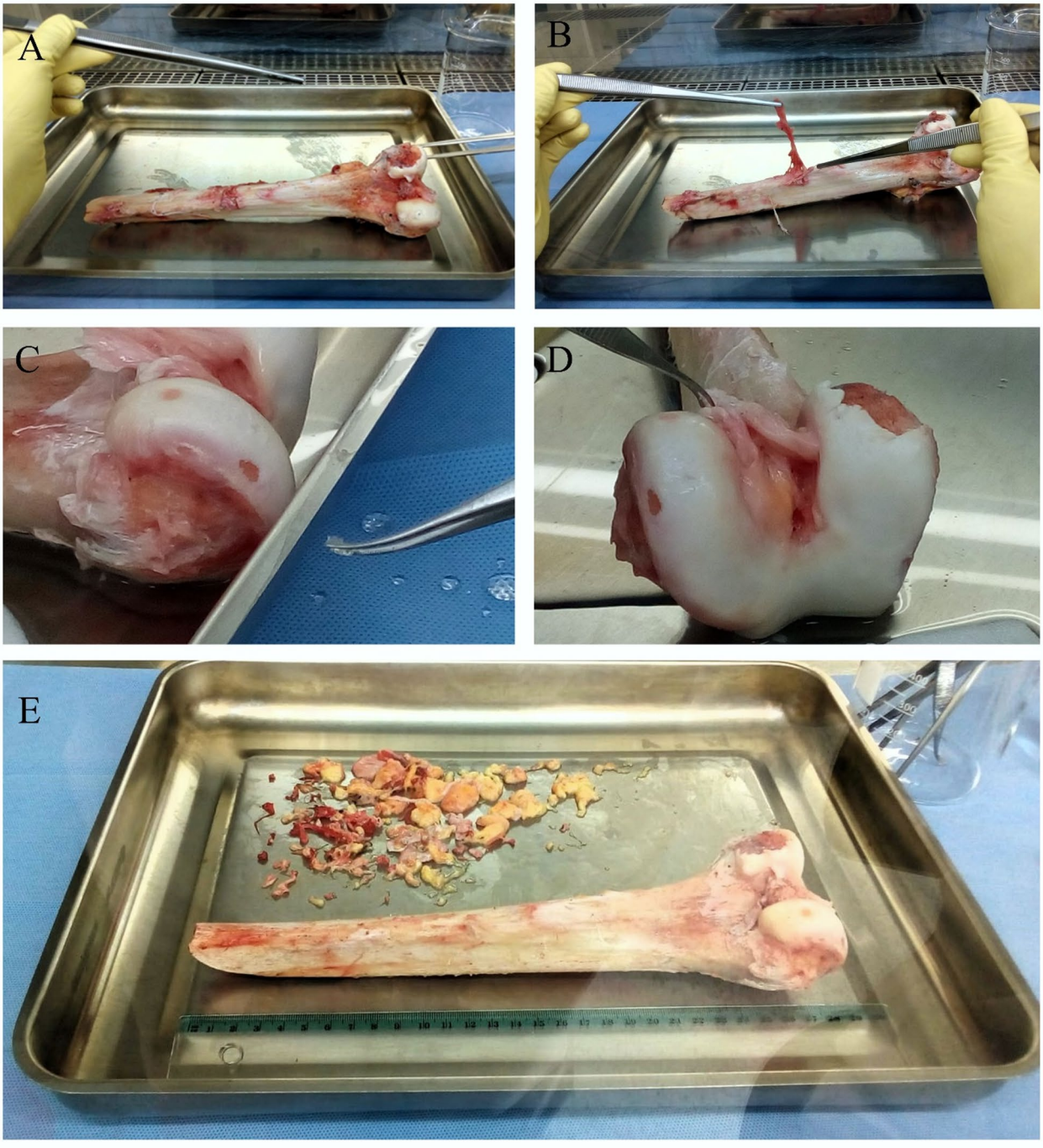

Fig. 1 Processing of a massive bone autograft. **A** Detailed graft debridement protocol: Bone graft (femur) before the cleaning, decontamination, and rinsing processes; **B** Cleaning of the bone and removal of excess connective tissue; **C** Removal of foreign debris, including glass, plastic, and asphalt residues, present on the bone due to trauma exposure; **D** Display of the condyle and the articular cartilage damage of the knee, along with a portion of the cruciate ligament; **E** After the cleaning process and the removal of excess connective tissue from the femur, the following procedures were carried out: measuring, pre-rinsing, decontamination and rinsing

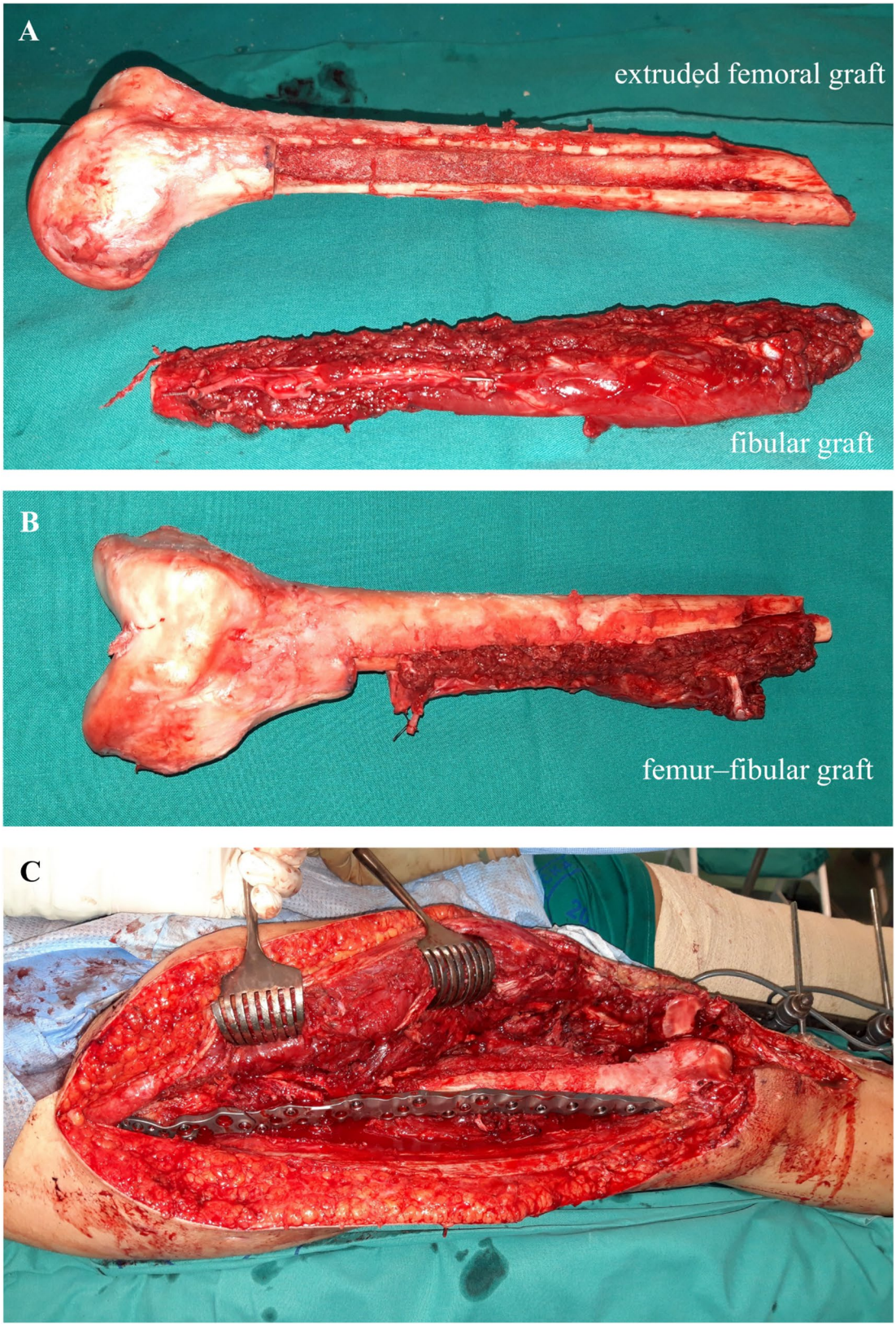

Fig. 2 Reconstruction and implantation of the femur–fibular graft. **A** The decontaminated femoral segment with the fibular graft before reconstruction; **B** The fibular graft was inserted into the medullary canal of the femoral segment, creating a femur–fibular composite graft; **C** Implantation was performed using a periprosthetic plate, ensuring stable fixation and preservation of the graft's vascular integrity

Testing, Storage, and Clinical Application of Musculoskeletal Tissue" was approved by the Ethics Committee of the Sestre milosrdnice University Hospital Centre (Approval No. 251-29-11/3-25-17). All procedures were conducted in compliance with the principles of the Declaration of Helsinki and the Guidelines for Good Clinical Practice. Written informed consent was obtained from all femoral head donors and from the patient prior to autologous clinical application.

The average age of the patients included in this study was 69 years (range: 55–81 years; three men and three women). Based on donor examination and evaluation, the tissues used in this research were deemed unsuitable for clinical use as allogeneic bone grafts. Femoral heads that were not approved for clinical use were utilized, for example, due to a positive serological finding for Anti-HBc (IgG + IgM), elevated inflammatory markers caused by urinary tract infection, or the presence of malignant disease in the donor. These exclusion criteria were not related to the histological or biological quality of the bone tissue and therefore are not expected to have influenced the study outcomes. Donor blood samples were tested for transmissible infections or diseases (HIV, HBV, HCV and *Treponema pallidum*) to prevent transmission to recipients. Additionally, microbiological analyses, including femoral head swabs and biopsies, were conducted to detect potential contamination.

Small bone grafts as a model for validating decontamination methods

Freshly frozen femoral heads ($n = 7$) obtained during the total hip replacement procedure in living donors were processed between April 2019 and December 2021. Microbiological control of the femoral heads was performed by swabbing, and microbiological results were sterile for all femoral heads included in the study. All bones were stored in appropriate sterile plastic containers (Freezable Tissue Storage Kit, Medfor, UK) in a quarantine freezer at -80 °C (Thermo Fisher Scientific) and had not undergone any processing prior to the validation procedure. Each femoral head, clearly marked as intended for validation purposes, was kept separate from those designated for clinical use.

Measuring and cutting of femoral heads

For validation, we used seven femoral heads stored at – 80 °C (35 bone fragments): six femoral heads were cut into 30 bone fragments and used for decontamination, microbiological sterility and for analysis of antibiotic residue, while one femoral head was cut into five fragments for cytogenesis assays. After thawing, the diameter (d) of each femoral head was measured before being divided into five fragments of approximately equal dimensions. One of the five fragments was immediately placed in a separate sterile plastic container and later used for microbiological analysis as a negative control (5/5). The remaining four fragments (1/5, 2/5, 3/5, and 4/5) were returned to the original container in which the bone was initially stored (Fig. 3). During the entire process of measuring and cutting bones in the operating room, air cleanliness was monitored using a Trypcase soy 3P® agar (TSA3) settle plate.

Transportation

Containers with bone fragments were sealed in a sterile zip bag and placed in a temperature-controlled transport box with cooling inserts and a moderate thermometer. The fragments were transported from the operating room at the Department of Traumatology to the Department of Microbiology at the Croatian Institute for Transfusion Medicine. During transit, the temperature was maintained between 4 °C and 8 °C, ensuring optimal transport conditions and preserving the quality and integrity of the fragments. To verify that the required temperature was consistently maintained, a wireless temperature datalogger (Mini SPY RF Green, Fesches le Châtel, France) was used to record temperature data throughout the transportation process.

Decontamination and rinse protocol

A total of five bacterial strains were used in this study. Three of them were reference strains from the National Collection of Type Culture (NCTC) and the National Collection of Pathogenic Fungi corresponding to strains from the American Type Culture Collection (ATCC: *Staphylococcus aureus* NCTC 10788/ATCC 6538, *Bacillus subtilis* NCTC 10400/ATCC 6633, and *Clostridium sporogenes* NCTC 532/ATCC 19404. Additionally, two more isolates were incorporated: *Staphylococcus epidermidis*, an environmental isolate, and *Cutibacterium acnes*, which was isolated from a patient's skull bone.

In this study, certified nutrient media were used, including Count-Tact® 3P® agar (CT3P), TSA3, Tryptic soy agar, Thioglycollate broth with resazuin (THIO-T), and Trypcase soy broth (TSB-T). Additionally, BacT/ALERT culture bottles with nutrient media and antibiotic neutralizers for aerobic (FA Plus) and anaerobic (FN Plus) microbial cultivation were used in the BacT/ALERT 3D (BioMérieux, France) automated colorimetric microbial growth reading system. All media and culture bottles were purchased from BioMérieux, France. The intentional contamination, pre-rinsing, decontamination, and rinsing of bone fragments were performed within a microbiological safety cabinet class II (Klimaoprema, Croatia) in an accredited microbiology laboratory at the Department of Microbiology, Croatian Institute of Transfusion Medicine, Zagreb, Croatia. Contamination of femoral head fragments was achieved by immersing four

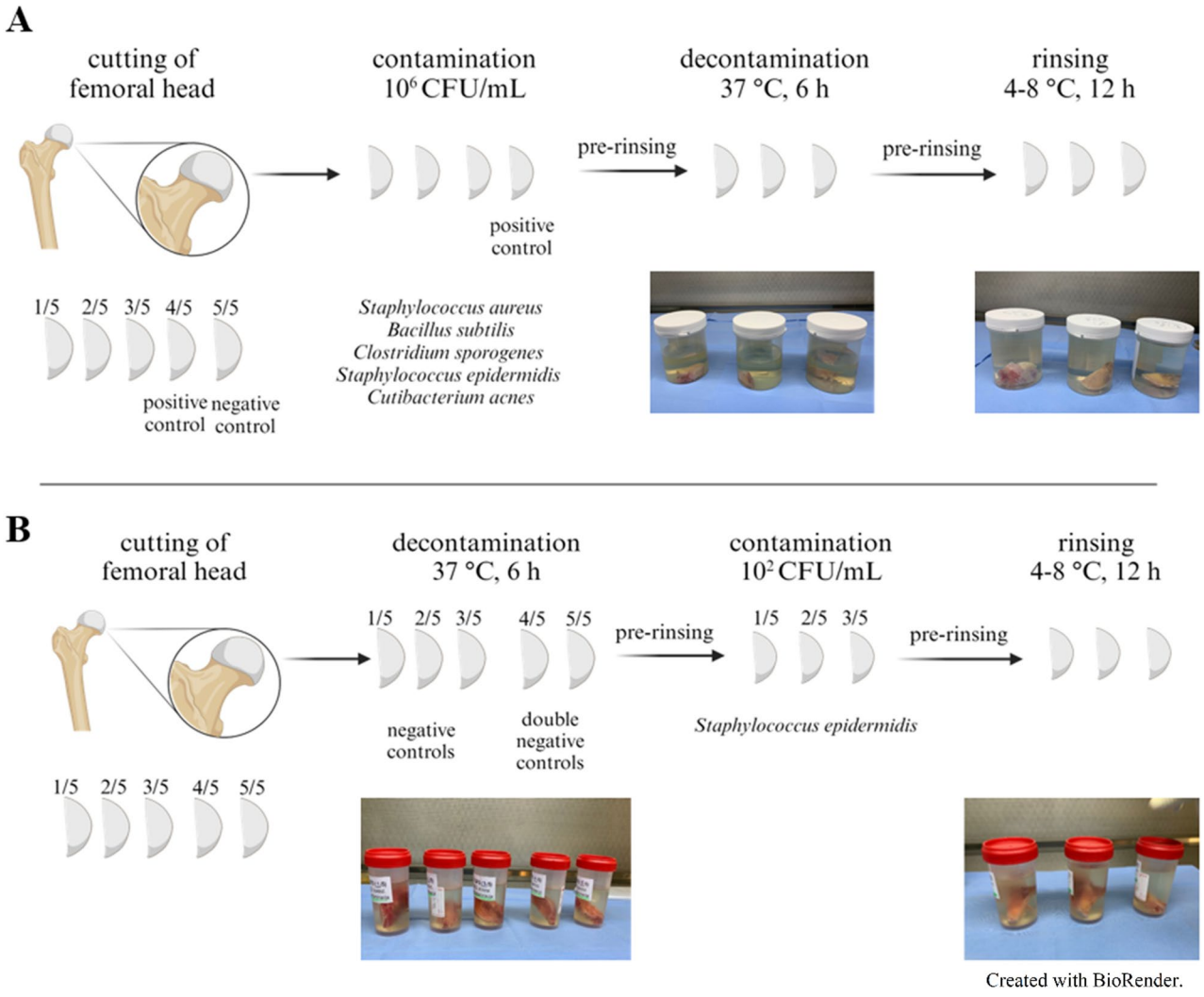

Fig. 3 Validation protocol for decontamination. **A** Experimental design scheme of decontamination: Six femoral heads were divided into five equal parts (1/5, 2/5, 3/5, 4/5, and 5/5), resulting in a total of 30 bone fragments used for the validation of decontamination. Four fragments from each femoral head (1/5, 2/5, 3/5, and 4/5) were intentionally contaminated with specific strains of microorganisms (*Bacillus subtilis*, *Clostridium sporogenes*, *Staphylococcus epidermidis*, *Staphylococcus aureus*, and *Cutibacterium acnes*) at a concentration of 10^6 CFU/mL. The decontamination process was performed on three bone fragments (1/5, 2/5, 3/5) from each femoral head using BASE 128 medium for 6 hours. These fragments were subsequently rinsed overnight in BASE medium to remove antibiotic residues. Bone fragments labeled 4/5 served as positive controls, while fragments labeled 5/5 were used as negative controls; **B** Controlled tissue contamination procedure scheme: A schematic representation illustrates the process wherein one femoral head is divided into five parts (1/5, 2/5, 3/5, 4/5, and 5/5). Although all the fragments were initially sterile, decontamination of these fragments was carried out as described above. After decontamination and rinsing, fragments 1/5, 2/5, and 3/5 were contaminated with *Staphylococcus epidermidis* at a low concentration of 10^2 CFU/mL and exposed to air for 15 min. Turbidity was observed in the medium on the second day of incubation, and identification tests confirmed the presence of *Staphylococcus epidermidis*. Fragments 4/5 and 5/5 were not contaminated and served as double negative controls, which remained sterile until the end of the prescribed incubation period. Image created with BioRender

fragments (labeled 1/5, 2/5, 3/5 and 4/5) from each femoral head into 150 mL of physiological solution containing a specific microorganism at a concentration of 10^6 CFU/mL [38]. Three intentionally contaminated fragments from each femoral head (labeled 1/5, 2/5, and 3/5) underwent decontamination and rinsing. Fragments 4/5 from each femoral head were directly inoculated into a liquid nutrient medium to serve as a positive control, while fragments 5/5 served as a negative control, as previously described (Fig. 3).

Decontamination process This process began with a brief pre-rinse in 1 L of physiological solution. Each fragment was subsequently decontaminated individually in a plastic container with 250 mL of BASE 128 medium at 37 °C for 6 h. BASE 128 medium (Alchimia Srl, Italy) was utilized for its efficacy decontaminating various human tissues intended for transplantation, including cardiovascular tissues, amniotic membranes, musculoskeletal tissues, tendons, and skin. This

medium contains vancomycin, gentamicin, cefotaxime, and amphotericin B deoxycholate. It should be stored at -20 °C and must be thawed and warmed to 37 °C before use (Fig. 3).
Rinsing process A brief pre-rinse in 1 L of physiological solution was performed after decontamination. Each fragment was then rinsed in a plastic container with 500 mL of BASE medium at 4 °C overnight. In subsequent iterations, the same procedure was repeated for each bone fragment, with an increased volume of saline solution used for pre-rinsing, decontamination medium, and rinsing medium. This increase in volume was designed to ensure thorough decontamination and rinsing while maintaining sterility and quality. BASE medium (Alchimia Srl, Italy) was used to rinse the bone tissues and remove antibiotic residues. In accordance with the manufacturer's recommendations, effective bone decontamination was achieved at 37 °C for 6 h, while rinsing was accomplished at 4–8 °C overnight. Both BASE 128 and BASE media are sterile and free of pyrogens and mycoplasmas, in compliance with current regulations in the European Pharmacopoeia [39] (Fig. 3).

Sterility testing of bone fragments after decontamination and rinsing procedures, as well as sterility testing of the final decontamination/rinsing fluid, was performed in a class A environment in accordance with the European Pharmacopoeia [39]. Each decontaminated bone fragment was inoculated in 150 mL of THIO-T and cultured in incubators (Selecta, Spain) at 37 °C. The turbidity of the broth was visually monitored daily for a total of 14 days of incubation. The final rinsing fluid from each bone fragment was inoculated into FA Plus and FN Plus bottles which were incubated for 14 days at 37 °C in BacT/ALERT 3D.

Assessment of antibiotic residues through controlled tissue contamination

To assess the presence or absence of antibiotic residues in order to prevent false negative results, a controlled contamination procedure was performed using *Staphylococcus epidermidis*, a representative of coagulase-negative staphylococci and the most common environmental contaminant. The femoral head was divided into five equal parts (1/5, 2/5, 3/5, 4/5, and 5/5). Although all the fragments were initially sterile, they were decontaminated in BASE 128 medium for 6 h at 37 °C, followed by an overnight rinse with BASE medium at 4–8 °C. Fragments 1/5, 2/5, and 3/5 were subsequently contaminated with *Staphylococcus epidermidis* at a low concentration of 10^2 CFU/mL and exposed to air for 15 min. Fragments 4/5 and 5/5 were not contaminated and served as negative controls. All fragments were then subjected to sterility testing [40] to evaluate the effectiveness of the decontamination and rinsing procedures.

Agar diffusion test for antibiotic residue analysis

Antibiotic residue analysis was performed using the agar diffusion test in duplicate on the fluid obtained after the final rinsing of each bone fragment [40]. Briefly, 2 mL of bacterial inoculum at a concentration of 10^6 CFU/mL was added to 38 mL of tryptic soy agar, thawed, cooled to approximately 45 °C, and poured into 120 × 120 mm plates using the pour plate method. Nine round wells with a diameter of 7 mm were made on each plate. Then, 100 µL of each tested sample of rinsing fluid was dripped into at least two wells on two different plates for each microorganism. BASE 128 medium was added dropwise to one well of each plate as a positive control.

Geometric analysis of bone fragments

To estimate the volume and surface area of the bone fragments, geometric calculations were performed. It was assumed that the femoral head approximates an ideal sphere, allowing for standard formulas to be used in the calculations.

Femoral head volume and surface area

The volume (V) and surface area (P) of each femoral head were calculated based on the measured diameter before cutting. The following formulas, assuming a spherical shape, were applied:

$$\mathrm{V} = \frac{4}{3} r^3 \pi \qquad \mathrm{P} = 4r^2 \pi$$

where r represents the radius of the femoral head and where π is approximately 3.14159.

Small bone fragments volume and surface area

This study analyzed 35 bone fragments obtained from seven femoral heads. The dimensions, surface areas, and volumes of these fragments were determined using the measured and calculated values of the femoral heads. To estimate the volume (V) and surface area (P) of one bone fragment, the following formulas were used:

$$\mathrm{V} = \frac{2}{3r^2 w} \qquad \mathrm{P} = 2\mathrm{rw} + \mathrm{r}2\pi$$

where w represents the width of the fragment.

Large bone autograft volume and surface area

To calculate the volume (V) and surface area (P) of one large femoral fragment, the following equations were applied:

$V = \frac{1}{3}hd^3\pi + \frac{1}{4}bd^2\pi L \quad P = 2hd^2\pi + bd\pi L.$

where h is the height, d is the diameter, b is the base width, and L is the length of the fragment.

Using these formulas, the geometric properties of the bone fragments were precisely calculated, allowing reliable estimations of their volume and surface area. The volume (V) is expressed in cubic centimeters (cm^3) or milliliters (mL), while surface area (P) is given in square centimeters (cm^2).

Histology and morphology

To better analyze the morphology of the bone fragments and the viability of osteoblasts and osteocytes, two fresh bone fragments and two frozen fragments after decontamination were embedded in paraffin. A routine laboratory tissue processing procedure, which is standard in pathohistological laboratories, was used. In brief, the process includes decalcification, embedding in paraffin, and cutting of histological slides. As a control, fresh bone processed in the same way was used. Processing the bone to embed it in paraffin requires that all bone fragments have undergone a decalcification process. Decalcification is performed because of the need to soften the bone for later cutting of histological tissue slides. The bone fragments are decalcified in a decalcification solution with formalin (Osteofast 1; Ref. No. OF1OT, Biognost, Croatia). The Osteofast solution was diluted with 10% buffered formalin in a ratio of 1:5, and bone fragments were immersed in such a solution for up to 24 h with continuous monitoring of the bone softening process. After adequate decalcification, the bone fragments were left in 10% buffered formalin for another 24 h. After that, the samples were processed in a histokinet and embedded in paraffin by routine procedure. During processing in a histokinet (automated tissue-processing device), the bone is dehydrated through an ascending alcohol series and cleared through substituted xylene, after which it is embedded in paraffin blocks. In the preparation of histological slides, paraffin-embedded bone fragments were cut into 2–3 μm thick sections, spread onto slides, and stained with hematoxylin and eosin (H&E). Through histological examination, the pathologist monitored the preservation of the bone structure and the presence of osteocytes and osteoblasts and thus the vitality of the bone tissue.

Cytogenesis - Comprehensive characterization of cells derived from bone

Isolation and morphological characterization of cells cultivated in vitro

The femoral head, obtained following a hip replacement procedure with the patient's informed consent, was cut into five equal fragments in the operating room and transported to the Tissue and Cell Bank. Further processing was carried out in a microbiological safety cabinet, where each fragment was labeled with a number from 1 to 5. Fragment 1, designated the fresh sample and underwent immediate processing, including the removal of connective tissue and fragmentation of both spongy and cortical parts of the bone. To facilitate the release of viable cells, the tissue was subjected to enzymatic digestion with collagenase II (0.42 mg/mL (100 IU/mL), Gibco, Life Technologies, USA) at 37 °C for six hours. Following this period, enzymatic activity was neutralized by adding cell culture medium, and the suspension was centrifuged (centrifuge 5810 R, Eppendorf, Germany) for four minutes at 1100 rpm at 4 °C. The resulting pellet was seeded into 75 cm^2 culture flasks containing DMEM (Dulbecco's modified Eagle medium, Life Technologies Europe BV, Netherlands) supplemented with 10% fetal bovine serum (FBS, Life Technologies, USA), 1% antibiotic-antimycotic (Life Technologies Europe BV, Netherlands), and 1% L-glutamine (Life Technologies Europe BV, Netherlands). The cells were cultured in an incubator at 37 °C in a 5% CO_2 atmosphere, and the media was changed every three to four days. To evaluate the effects of deep freezing on the growth and proliferation of isolated cells, fragments 2 and 4 were frozen in 10% DMSO freezing medium (Sigma–Aldrich, USA) and stored at -80 °C, while fragments 3 and 5 were placed in an empty container without a cryoprotectant and kept at the same temperature. The first group of deep-frozen fragments (2 and 3) remained frozen for 15 days, whereas the second group (4 and 5) was stored for 30 days. After the designated storage periods, the containers were removed from the freezer and left to thaw at room temperature. Post-thaw processing varied depending on the presence of DMSO. Fragments previously frozen with the cryoprotectant were subjected to four sequential washes in physiological saline solution (B. Braun, Germany), each lasting 10 min, to eliminate any residual DMSO before enzymatic digestion. In contrast, those preserved without a cryoprotectant proceeded directly to digestion without rinsing. Subsequent processing, including enzymatic digestion and cell seeding, followed the same protocol established for the fresh bone fragments. Throughout the study, cell growth, confluence, and morphological characteristics were observed using a Nikon Eclipse Ti U microscope (Nikon, Japan) before each media change.

Cell counting, viability and cumulative population doubling time

For cell counting and viability determination, the LUNA-FX7 (Logos Biosystems, South Korea) automated cell counter with the corresponding counting slides was used. According to the manufacturer's instructions, the analysis was performed in fluorescence mode using the fluorescent dyes acridine orange and propidium iodide.

Before counting the cell cultures, device validation was performed using a validation slide to ensure measurement accuracy. Upon completion of the counting process, a quality control graph was generated, confirming that the results fall within the acceptable range compared to the reference values obtained during the validation slide registration. During cell counting, the sample and fluorescent dyes (acridine orange/propidium iodide) were mixed in a 9:1 ratio. Before loading onto the slide, the prepared sample was gently resuspended, and 10 µL of the sample was applied to the appropriate chamber of the counting slide. After loading, live and dead cells are clearly visible on the device display. The cumulative population doubling (cPD) and doubling time (DT) were calculated when the cells reached 80% confluence. The calculation was performed using the following formula:

$$cPD = \ln\frac{N}{\mathrm{N0}}x3.322$$

$$DT = \frac{\mathrm{CT}}{\mathrm{cPD}}$$

where N is the number of live cells, N_0 is the initial number of seeded live cells, and CT is the total culture duration in days.

Holographic time-lapse imaging

Osteoblasts were isolated from five femoral head fragments, one of which was fresh, while other four underwent different deep-freezing protocols. Cells were seeded at a density of 30 000 cells per well in a standard tissue culture-treated 6-well polystyrene plate (Sarstedt, Germany). Holographic time-lapse imaging was performed using the Holomonitor M4 digital holographic cytometer (Phase Holographic Imaging, PHI, Sweden) placed in an incubator at 37 °C with 5% CO_2. Cells were imaged at 10 different positions per well for 5 days (120 h), and images were captured every 10 min. Time-lapse phase imaging, image processing and single-cell tracking analysis were performed using Hstudio software (PHI).

Hematoxylin-eosin staining

The suspension of the cells was smeared on the slides and air-dried for two days. Fixation was performed by immersing the slides in ice-cold acetone (CLARO-PROM, Croatia) for four minutes at room temperature, followed by rinsing in DPBS (Dulbecco's phosphate buffer saline, Dako, Denmark) buffer. The slides were subsequently rinsed with distilled water and immersed in a hematoxylin solution (Sigma-Aldrich®, USA) diluted 1:5 in distilled water. After two minutes, the slides were removed from the hematoxylin and rinsed with both distilled water and running water. The samples were immersed in concentrated eosin (Sigma-Aldrich®, USA) for one minute, followed by another rinse in distilled water. For mounting, the slides were dehydrated by sequential immersion in ethanol (Etil promet, Croatia) at increasing concentrations from 70% to 100%, each for one minute. This was followed by immersion in a xylene substitute (Tissue-Tek®, Netherlands). Finally, the slides were covered with a mounting solution (Tissue-Tek®, Netherlands) and a coverslip. The cell morphology was observed under a microscope (APX100 digital imaging system, Olympus, Japan) and imaged using a camera (DP23, Olympus, Japan).

Immunocytochemical detection of Ki67 expression

The proliferation index was determined by counting Ki67-positive cells under the inverted digital microscope (Mateo, Leica). For immunocytochemical staining, cells were seeded onto positively charged slides designed for immunohistochemical (IHC) staining (FLEX IHC microscope slides, Dako, Denmark). Each slide was seeded with 20 000 cells, and four slides were prepared for each of the five samples. A total of 250 µL of cell suspension was pipetted onto each slide, followed by a two-hour resting period to allow initial attachment. After this incubation, a nutrient cell medium was added to cover the entire surface of the slide. The slides were then placed in an incubator at 37 °C with 5% CO_2 for 24 h to ensure cell adhesion. Prior to IHC staining, slides were air-dried for one day, and fixation was performed by immersing the slides in ice-cold acetone (CLARO-PROM, Croatia) for four minutes at room temperature, followed by rinsing in DPBS (Dako, Denmark) for up to two minutes.

A positive IHC reaction was visualized as brown staining in nuclei containing the Ki67 protein. Ki67-positive cells were counted under the microscope (APX100 digital imaging system, Olympus, Japan), and a digital camera was used (DP23, Olympus, Japan). The proliferation index was calculated by dividing the number of Ki67-positive cells by the total number of cells counted. Counting was performed in eight fields of view at low magnification (100 ×), and the process was repeated twice. Prior to the IHC reaction, cell or tissue preparation was necessary. Since a primary antibody was used to detect the Ki67 protein located in the nucleus, it was necessary to enable the antibody to penetrate through the cell membrane. Antigen retrieval was achieved by boiling the cells in citrate buffer at neutral pH (Dako, Denmark) at 96 °C for 20 min in a water bath (NB 5, Nuve, Turkey). After boiling, the slides were cooled to room temperature for at least 20 min and then rinsed with DPBS. Following rinsing, the slides were removed from the buffer, and the area surrounding the marked region was wiped. A total of 70 µL of the primary antibody for Ki67 (clone MIB1, mouse monoclonal, Dako, Denmark) at a concentration of 5 ng/

µL was pipetted onto each sample. The slides were then incubated in a humid, dark chamber for 30 min at room temperature. Afterward, the slides were rinsed by immersion in a DPBS tray, and 70 µL of secondary antibody (goat anti-mouse EnVision Flex, Dako, Denmark) was added and incubated for 30 min at room temperature. Another rinse in DPBS was performed before 70 µL of 3,3'-diaminobenzidine chromogen (Dako, Denmark) was added, with a 10 min incubation at room temperature before a final rinse with distilled water. Counterstaining was performed by immersing the samples in hematoxylin (Sigma–Aldrich®, USA) diluted 1:5 in distilled water for two minutes at room temperature, followed by rinsing in distilled and tap water. To ensure long-term preservation, the slides were dehydrated by sequential immersion in ethanol (Etil promet, Croatia) at increasing concentrations from 70% to 100%. After rinsing, ethanol was replaced with a xylene substitute (Tissue-Tek®, Netherlands), and a mounting solution (Glas™ Tissue mount™ Tissue-Tek®, Sakura Finetek, Netherlands) was applied to the slides, followed by the addition of coverslips.

Immunophenotyping and cell viability via flow cytometry

For sample preparation and staining, 300 µL of cell suspensions at a concentration of 1×10^6 cells/mL were separated into individual tubes and washed with 2 mL of DPBS (Sigma–Aldrich, USA) to remove the culture medium. After the removal of DPBS, 5 µL of the previously prepared Live/Dead stain was added to the cells, and the samples were incubated for 20 min in the dark at room temperature. The Live/Dead stain was prepared by adding 3 µL of Live/Dead fixable stain (Thermo Fisher, USA) to 57 µL of ultrapure water (obtained from the Select Fusion 160 device, Suez, France). After resuspension, 5 µL of the diluted stain was taken from the 60 µL mixture and further diluted in 100 µL of the cell suspension in DPBS, resulting in a final dilution of 400 ×. Following incubation, the samples were washed with 2 mL of DPBS and centrifuged for 5 min at 500 × g at room temperature, after which the cell pellet was resuspended in 100 µL of DPBS. The suspension was then transferred to a pre-formulated DURAClone SC Mesenchymal Tube (Beckman Coulter, USA) and incubated for 15 min at room temperature in the dark. The tubes contained a dried antibody panel for the detection of a total of nine surface markers (CD14, CD19, CD31, CD34, CD45, CD73, CD90, CD105, and CD146), among which CD34, CD31, CD73, CD90, CD146, and CD105 were observed on the analyzed cells. Next, the samples were incubated for 10 min at room temperature in VersaLyse reagent (Beckman Coulter, USA), protected from light, and centrifuged for 5 min at 500 × g (RT), after which the cell pellet was resuspended in 500 µL of a 0.1% aqueous paraformaldehyde solution (Electron Microscopy Sciences, USA) in DPBS. Finally, the samples were analyzed using a flow cytometer (DxFlex, Beckman Coulter, USA). The final data processing was performed using FlowLogic software (Inivai Technologies, Australia). During analysis, cell aggregates, CD45-positive cells (expressed only on the surface of leukocytes) [41], and non-viable cells were excluded from the analysis and data processing.

Immunofluorescence

Osteoblasts were plated at a density of 20 000 cells per 3.5 cm glass-bottom dishes (MatTek, #1.5 coverglass) and cultured in a humidified Galaxy 170 S incubator (Eppendorf, Germany) at 37 °C and 5% CO_2. Cells were maintained in DMEM (Thermo Fisher, Cat# 11995065) containing 1 g/L D-glucose, pyruvate, and L-glutamine, supplemented with 10% heat-inactivated fetal bovine serum (FBS; Sigma-Aldrich) and a standard penicillin (100 IU/mL)/streptomycin (100 µg/mL) antibiotic mix (Lonza). To capture mitotic stages, cells were fixed at room temperature for 10 min using a fixative composed of 4% paraformaldehyde (PFA) and 0.2% glutaraldehyde (GLA). For RUNX2 immunostaining, fixation was done using only 4% PFA. After fixation, cells were rinsed three times in DPBS, five minutes per wash. Membrane permeabilization was carried out using 0.5% Triton X-100 in DPBS for 15 min. Following this, cells were incubated with 1% normal goat serum in PBS at 4 °C for one hour to block nonspecific antibody binding. Primary antibodies diluted in 1% normal goat serum were added and incubated overnight at 4 °C. The antibodies used included rat anti-α-tubulin (Invitrogen MA1-80017, 1:300) and mouse anti-RUNX2 (Abcam ab76956, 1:100). The next day, cells were washed three times with DPBS and incubated with secondary antibodies (in 2% normal goat serum) for one hour at room temperature. Secondary antibodies included Alexa Fluor 488 goat anti-mouse IgG (Abcam ab150113, 1:250) and Alexa Fluor 594 donkey anti-rat IgG (Abcam ab150156, 1:500). Finally, cells were counterstained with 100 nM SiR-actin (Spirochrome) and 1 µg/mL 4′,6-diamidino-2-phenylindole (DAPI) for 20 min to label the actin cytoskeleton and DNA, respectively.

Imaging

Imaging was performed using a Zeiss laser scanning 800 confocal microscope equipped with an Airyscan Superresolution module and mounted on an Axio Observer. Z1 inverted platform (Carl Zeiss, Germany). For mitotic spindles, multi-plane (z-stack) imaging was used to capture the full spindle volume. Excitation wavelengths were 405, 488, 561, and 640 nm for DAPI, Alexa Fluor 488, 594, and SiR, respectively. Image acquisition was done with Plan-Apochromat 63×/1.40 Oil differential interference contrast M27 or Plan-Apochromat 40×/0.95 Corr M27 objectives. For interphase imaging, tile scanning and

z-stack acquisition were performed using the 40×/0.95 Corr M27 objective. All images were collected using the Zeiss Efficient Navigation Blue 3.4 software (Carl Zeiss).

Image analysis

Quantitative image analysis was conducted in ImageJ/Fiji (National Institutes of Health, USA). Nuclear area was determined by manually outlining the DAPI-labeled DNA using the polygon selection tool. Nuclear RUNX2 intensity was measured from sum-intensity projections across all z-planes, using the DAPI signal to define nuclear boundaries in the RUNX2 channel. Background signal was measured in the cytoplasm (1 × 1 µm region) and subtracted from nuclear intensity values. The corrected integrated fluorescence intensity was then normalized by dividing by the number of z-planes used in the projection. Spindle length was quantified as the distance between spindle poles, identified by regions of high α-tubulin intensity. Spindle width was measured as the lateral distance between the two most distant kinetochore fibers, perpendicular to the pole-to-pole axis. All numerical analyses were performed in MATLAB (MathWorks). Statistical comparisons across groups used one-way ANOVA followed by Tukey's Honest significant difference post hoc test ($\alpha = 0.05$). Linear regression analysis, including R^2 and p-values, was carried out using the fitlm function in MATLAB. Figures were assembled using Adobe Illustrator CC (Adobe Systems).

Induction of osteogenic differentiation and evaluation of differentiation markers

Cells isolated from different bone fragments - fresh bone, bone frozen for 15 days in DMSO and bone frozen for 15 days without DMSO were seeded at a density of 56 250 cells/cm^2 in triplicates in 6-well plates for differentiation treatment. After seeding, the cells from bone fragments were cultured for 14 days in differentiation medium containing 50 µg/mL ascorbic acid (Sigma-Aldrich, SAD) and 4 mM β-glycerophosphate (Sigma-Aldrich, SAD), and the media was changed twice a week. After 14 days of treatment, RNA was extracted using the Quick-RNA Miniprep isolation kit (Zymo Research). Along with measuring RNA concentration, A_{260}/A_{280} and A_{260}/A_{230} ratios were measured to assess purity of RNA. Upon evaluation of RNA quality, the samples were treated with RNase-free DNAse I (Thermo Fisher Scientific) to remove residual genomic DNA. DNase-treated RNA samples were then reverse transcribed using the iScript cDNA synthesis kit (Bio-Rad), including a no-reverse transcription control, to assess residual genomic DNA in downstream experiments. Quantitative PCR (qPCR) was performed using primers for alkaline phosphatase (gene *ALPL*) and collagen type I (gene *COL1A1*), while actin β (gene *ACTB*) served as the endogenous control. The qPCR was set up using SsoAdvanced™ Universal SYBR® green supermix (Bio-Rad) under the following conditions: initial denaturation at 95 °C for 30 s, followed by 40 cycles of 95 °C for 15 s and 60 °C for 1 min. No-template controls were included for all primer pairs. Melting curve analysis was performed by increasing the temperature in 0.5°C increments from 65°C to 95°C, and qPCR was performed the CFX Opus 96 Real-Time PCR system (Bio-Rad). The primer pairs used were obtained from Origene (www.origene.com) and are as follows (5' –>3'):

ALPL Fw: GCTGTAAGGACATCGCCTACCA, Rev: CCTGGCTTTCTCGTCACTCTCA;

COL1A1 Fw: GATTCCCTGGACCTAAAGGTGC, Rev: AGCCTCTCCATCTTTGCCAGCA;

ACTB Fw: CACCATTGGCAATGAGCGGTTC, Rev: AGGTCTTTGCGGATGTCCACGT.

The data were analyzed using the ddCq method to determine relative gene expression and are presented as the average of three values and standard deviation. Statistical analysis was performed using Welch t test, with a p value < 0.05.

Von Kossa staining

The von Kossa staining method was used to detect calcium mineral deposition in cells, serving as a marker of late-stage osteogenic differentiation. Cells were cultured following the same protocol as for gene expression analysis (qPCR). On day 21 after seeding, the culture medium was removed, and the cells were washed twice with 1 mL DPBS. Cells were then fixed with 1 mL of 4% paraformaldehyde (Sigma-Aldrich, USA) for 5 min and washed twice with distilled water (deH_2O). A 2% silver nitrate solution (2 g $AgNO_3$ dissolved in 100 mL deH_2O; Kemika d.d., Croatia) was added, and cells were incubated for 1 h at room temperature (RT). After incubation, the solution was discarded, and cells were washed twice with deH_2O. Subsequently, cells were treated for 5 min with 1 mL of 2.5% sodium thiosulfate pentahydrate solution (2.5 g $Na_2S_2O_3 \cdot 5\ H_2O$ in 100 mL deH_2O; T.T.T., Croatia) and washed twice with deH_2O. Stained samples were examined under light microscopes Olympus BX51 (Olympus, Japan) and Zeiss HBO 50/AC (Zeiss, Germany).

Microarray analysis

Genomic DNA was extracted from five samples using the PureLink™ Genomic DNA Mini Kit (Invitrogen, Carlsbad, CA, USA) according to the manufacturer's protocol. Molecular karyotyping was performed using the SurePrint G3 Human comparative genomic hybridization (CGH) 8 × 60 K microarray platform with an average probe spacing of 41 kb (Agilent Technologies, Santa Clara, CA, USA). Data were analyzed using Agilent Cytogenomics software (Agilent Technologies, Santa Clara, CA, USA) with reference to the human genome

assembly GRCh38 (hg38). Results were interpreted and described according to the ISCN 2024 guidelines.

Results

Sterility after decontamination of massive autograft

Here, we present the results of the decontamination and rinsing of a massive bone autograft at the Tissue and Cell Bank. As previously described, the graft was accidentally ejected from the body of a 24-year-old patient as a result of a car accident (Fig. 1). Initial microbiological analysis of the bone swab and transport medium revealed contamination. *Bacillus* spp. and *Streptococcus mitis* were isolated from the bone swab, while the transport medium contained coagulase-negative staphylococci (CoNS), *Bacillus* spp., and *Streptococcus mitis* (Table 1).

Successful cleaning of the autologous bone was achieved, with complete removal of excess connective tissue and foreign debris such as glass, plastic, and asphalt residues resulting from the traumatic exposure. Proper visualization of the condyle, articular cartilage damage, and a portion of the cruciate ligament was ensured which was necessary for successful reimplantation of femur. Decontamination of the bone was performed following pre-rinsing, in accordance with optimized protocols (see Methods). Following the decontamination procedure, microbiological testing confirmed the sterility of the swab, decontamination fluid (Base 128), rinsing fluid (BASE) and soft tissue near the bone (aerobic and anaerobic cultivation) (Table 1). The successful decontamination, confirmed by sterile microbiological results, ensured the safe reimplantation of the graft during a surgical procedure performed at the Clinic for Traumatology, Sestre milosrdnice University Hospital Center (data not shown).

Clinical results and case follow-up

The baseline condition, which includes preliminary resuscitation and debridement followed by bridging external fixation, is shown in Fig. 4A. Postoperative radiographs demonstrated satisfactory alignment and stable fixation of the reconstructed femur (Fig. 4C, F). At four months postoperatively, the patient presented with mild anterior knee pain and stiffness, with a range of motion (ROM) of 0–40°. Arthroscopic arthrolysis and manipulation under anesthesia were performed, followed by removal of the patellar plate. Arthroscopic evaluation revealed well-preserved articular cartilage and fibrocartilaginous repair tissue at the posterolateral femoral condyle (Fig. 4B). After a structured physiotherapy program, knee motion improved to 0–87° at six months. At the one-year follow-up, the patient reported subjective knee instability. Clinical examination revealed a negative posterior drawer test, a markedly positive valgus stress test (+++), and a slightly positive varus stress test. Reconstruction of both the posteromedial and posterolateral corners was subsequently performed using semitendinosus and gracilis tendon grafts, respectively, following the Larson technique. Radiographs obtained one year after surgery showed complete fracture union, with evident hypertrophy and remodeling of the fibular graft (Fig. 4D, G). At that time, the patient was pain-free and demonstrated a functional knee ROM of 0–90°. Long-term radiographs obtained three years after surgery confirmed maintained alignment and graft remodeling (Fig. 4E, H).

Table 1 Microbiological results before and after decontamination of the femur

Time	Microbiological sampling	Results
Before	*Swab*	*Bacillus* spp; *Streptococcus mitis*
	Transport medium	CoNS; *Bacillus* spp; *Streptococcus mitis*
After	*Decontamination medium (FA)*	Sterile
	Decontamination medium (FN)	Sterile
	Rinsing medium (FA)	Sterile
	Rinsing medium (FN)	Sterile
	Swab	Sterile
	Biopsy of soft tissue (TSB-T)	Sterile
	Biopsy of soft tissue (THIO-T)	Sterile

Trypcase soy broth (TSB-T), thioglycollate broth with resazuin (THIO-T), bottles for aerobic (FA) and anaerobic (FN) cultivation

Sterility of small bone fragments, controlled tissue contamination, antibiotic residue, and histology

We analyzed the effectiveness of decontamination on small bone fragments and assessed the levels of residual antibiotics after treatment. To ensure consistency during the decontamination process, the bone fragments were collected and cut into uniform sizes (Methods). The method of pre-rinsing, decontamination, and final rinsing of bone tissue was found to be highly reliable in terms of avoiding false-negative or false-positive results. During the validation process, both negative and double-negative controls remained negative throughout the end of the prescribed incubation period, while positive controls predictably yielded positive results within the expected timeframe (Tables 1 and 2).

To remove any residues of disinfectants or contaminants, this step is crucial to ensure that the remaining antibiotic residues are minimized. Residual antibiotics in the rinsing medium were analyzed using the agar diffusion test (Fig. 5G). This test helps determine the presence of antibiotic residues by measuring the zone of inhibition around wells filled with the control medium (BASE 128) and the medium in which the bone fragments were rinsed overnight (BASE). The decontamination method was effective in reducing/removing antibiotics from the decontamination medium, resulting in a minimal zone of inhibition of 0 mm for *Staphylococcus aureus*, 4 mm

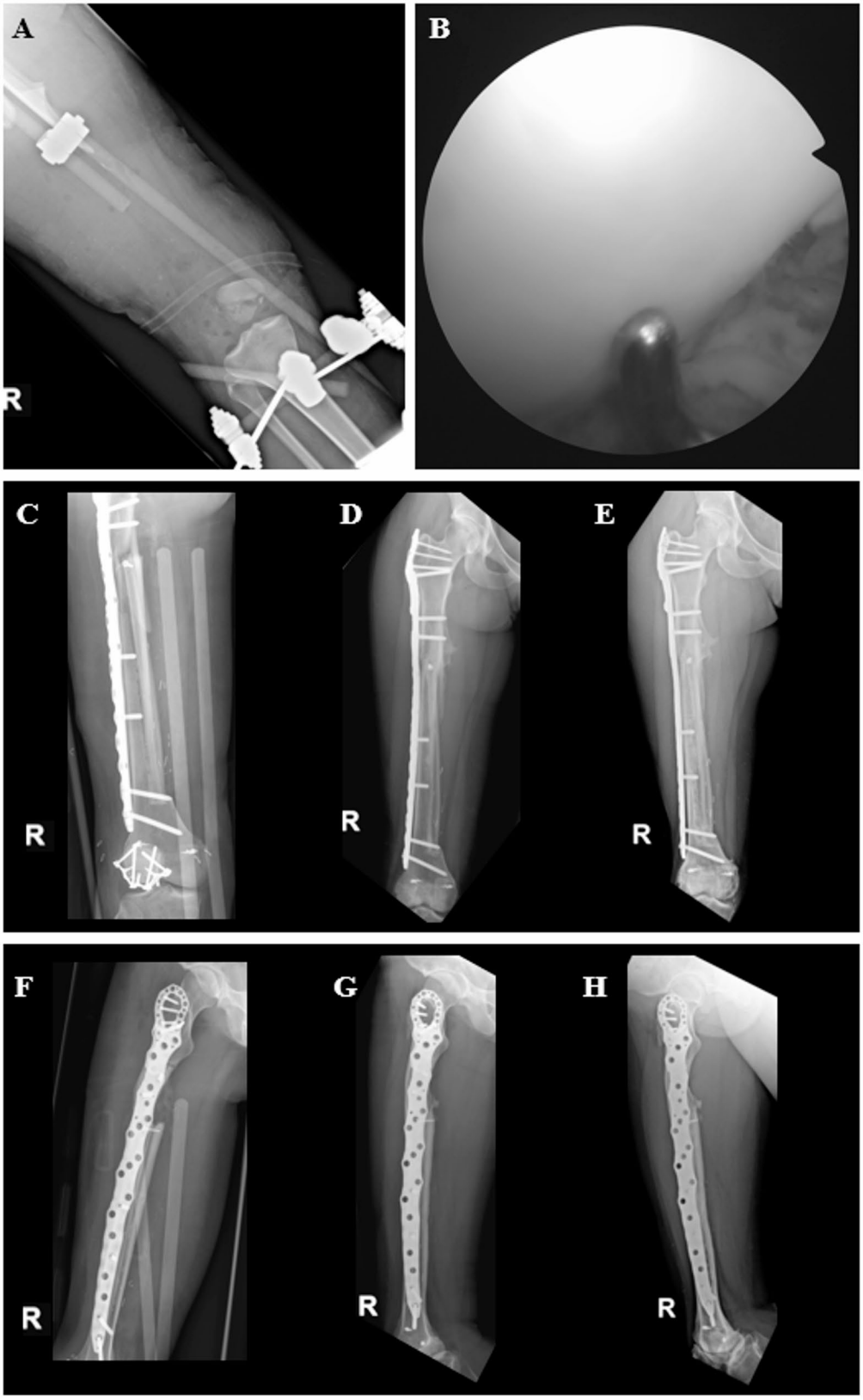

Fig. 4 (See legend on next page.)

(See figure on previous page.)

Fig. 4 Postoperative radiographic follow-up. **A** Baseline condition with preliminary resuscitation, debridement, and bridging external fixation; **B** Arthroscopic view at four months postoperatively showing preserved articular cartilage and fibrocartilaginous repair tissue at the posterolateral femoral condyle; **C**, **F** Postoperative radiographs demonstrating satisfactory alignment and stable fixation of the reconstructed femur; **D**, **G** Radiographs at one year postoperatively showing complete fracture union with hypertrophy and remodeling of the fibular graft; **E**, **H** Long-term follow-up at three years confirming maintained alignment and continued graft remodeling

for *Bacillus subtilis*, and 3 mm for *Staphylococcus epidermidis* (Fig. 5H). On the second day of incubation, after controlled contamination with *Staphylococcus epidermidis*, the medium exhibited turbidity, and identification tests confirmed the presence of *Staphylococcus epidermidis*. We demonstrated that the medium did not contain residual antibiotics at concentrations sufficient to inhibit possible bacterial growth, which is a prerequisite for reliable sterility testing.

Altogether, these findings confirm that the decontamination protocol is highly effective in eliminating bacterial contamination, both in a single massively contaminated bone fragment (*Bacillus spp*., *Streptococcus mitis*, CoNS) and in 30 bone fragments experimentally contaminated with various microbial strains (*Bacillus subtilis*, *Clostridium sporogenes*, *Staphylococcus epidermidis*, *Staphylococcus aureus*, and *Cutibacterium acnes*). The decontamination and rinsing procedure achieved a 100% success rate in reliably preserving bone tissue vitality, without leaving inhibitory levels of antibiotic residues.

Cytogenesis

Characterization of osteoblasts isolated from fresh versus frozen bone

Viability, proliferation and morphological analysis Inspired by the successful clinical autologous transplantation of a large bone frozen for 15 days without DMSO following decontamination and cleaning (data not shown), we hypothesized that frozen bones might retain populations of proliferating cells capable of regenerating and healing the displaced bone upon transplantation. To test this hypothesis, we isolated cells from spongy and cortical bone and performed morphology analysis in cell culture. To characterize them, we implemented a panel of molecular biology techniques. Cells isolated from fresh and frozen bone fragments present heterogeneous morphologies, including polygonal and spindle shapes as well as stellate morphologies. Some cells present long dendritic protrusions, as well as various lamellipodia and pseudopodia. We successfully isolated osteoblasts from bone fragments of fresh bone, as well as from bone fragments stored at -80 °C, both with and without DMSO, after 15 and 30 days. The first individual cells were obtained after 24 h through enzymatic digestion (see Methods), while another portion of the cells continuously and spontaneously emerged from the bone fragments of fresh bone. The cells from the frozen bone fragments began emerging after 72 h with individual cells also visible. After the initial isolation of osteoblasts from bone fragments in the primary passage (p0), a cell culture was established (see Methods). Confluence from fresh bone was achieved after 7–10 days of culture, whereas cell growth to 50–60% confluence from frozen bone fragments was achieved after 3–4 weeks. The cells continued to grow through secondary passages, while another portion of the cells was stored in liquid nitrogen at -196 °C. In secondary passages, cell proliferation and viability were higher than in the first passages: in p0 (after thawing from liquid nitrogen), the viability was 82.60% ± 4.92 while in p1, it was 97.64% ± 1.46; and in p4, it was 98.22% ± 1.65 (Fig. 6A). Additionally, we analyzed the morphological characteristics and proliferation indices of osteoblasts ($n = 2525$) on the seventh day after cultivation at p2 (Fig. 6B). Obtained results revealed osteoblasts with elongated and spindle-shaped forms, and with nuclei positive for the Ki67 protein. The nuclei of cells containing functional Ki67, a marker of active proliferation, were stained brown, whereas those of the remaining cells were stained with native hematoxylin. The osteoblasts isolated from fresh bone had 60% Ki67-positive cells, while osteoblasts isolated from frozen bone was 57.30% ± 1.30 (Fig. 6B). These findings support the hypothesis that frozen bone fragments retain viable, proliferating osteoblasts even after extended storage which is potentially due to the protective effect of the bone matrix.

Osteogenic potential of osteoblasts isolated from fresh* versus *frozen bone To explore the relationship between nuclear size and the expression of Runt-related transcription factor (RUNX2), an early marker essential for the osteogenic differentiation of MSCs into osteoblasts [42], was assessed in cell cultures (p1) established from fresh and frozen bone samples.

We established cell cultures from untreated fresh bone samples and from bone samples frozen at -80 °C with and without DMSO, the gold-standard cryopreservation agent [43] (Fig. 7A). After the cells were cultured, they were fixed and labeled with SiR-actin, DAPI, and RUNX2-specific primary antibodies conjugated with secondary antibodies coupled to a red dye (Fig. 7B, see also Methods). Multiple fields of view were imaged in 3D by fluorescence confocal microscopy (see Methods). The average RUNX2 level in the nucleus was quantified by calculating the average intensity of the RUNX2 signal in summed projections of z-plane images in individual cells (see Methods). The average nuclear size and RUNX2

Table 2 Microbiological results after decontamination of small bone fragments

Bone samples		**Fragments for decontamination**			**Fragment for positive control**	**Fragment for negative control**
Femoral head 1		**1/5**	**2/5**	**3/5**	**4/5**	**5/5**
Microorganism (10^6 CFU/mL)		*Bacillus subtilis*				/
Results	Bone – THIO-T	Sterile	Sterile	Sterile	Positive	Sterile
	Medium - FA	Sterile	Sterile	Sterile	/	/
	Medium - FN	Sterile	Sterile	Sterile	/	/
Femoral head 2						
Microorganism (10^6 CFU/mL)		*Clostridium sporogenes*				/
Results	Bone – THIO-T	Sterile	Sterile	Sterile	Positive	Sterile
	Medium - FA	Sterile	Sterile	Sterile	/	/
	Medium - FN	Sterile	Sterile	Sterile	/	/
Femoral head 3						
Microorganism (10^6 CFU/mL)		*Staphylococcus epidermidis*				/
Results	Bone – THIO-T	Sterile	Sterile	Sterile	Positive	Sterile
	Medium - FA	Sterile	Sterile	Sterile	/	/
	Medium - FN	Sterile	Sterile	Sterile	/	/
Femoral head 4						
Microorganism (10^6 CFU/mL)		*Staphylococcus aureus*				/
Results	Bone – THIO-T	Sterile	Sterile	Sterile	Positive	Sterile
	Medium - FA	Sterile	Sterile	Sterile	/	/
	Medium - FN	Sterile	Sterile	Sterile	/	/
Femoral head 5						
Microorganism (10^6 CFU/mL)		*Cutibacterium acnes*				/
Results	Bone – THIO-T	Sterile	Sterile	Sterile	Positive	Sterile
	Medium - FA	Sterile	Sterile	Sterile	/	/
	Medium - FN	Sterile	Sterile	Sterile	/	/
Bone samples		***Fragments for contamination***			***Fragments for double negative control***	
Femoral head 6		**1/5**	**2/5**	**3/5**	**4/5**	**5/5**
Decontamination and rinsing		Sterile	Sterile	Sterile	Sterile	Sterile
Microorganism (10^2 CFU/mL)		*Staphylococcus epidermidis*			/	/
Results	Bone – THIO-T	Positive	Positive	Positive	Sterile	Sterile
	Medium - FA	Positive	Positive	Positive	Sterile	Sterile
	Medium - FN	Positive	Positive	Positive	Sterile	Sterile

Colony-forming unit (CFU), thioglycollate broth with resazuin (THIO-T), bottles for aerobic (FA) and anaerobic (FN) cultivation

levels were then compared across different conditions, and the correlation between nuclear size and RUNX2 intensity was also assessed.

Interestingly, under all conditions except after 30 days of freezing in DMSO, the cells were, on average, positive for RUNX2 (Fig. 7B and C). These findings suggest that cells isolated from frozen bone fragments are able to proliferate and differentiate in culture after freezing. A higher average level of RUNX2 was observed in the population of cells isolated from fresh and frozen bone fragments for 15 days, irrespective of the presence or absence of DMSO (Fig. 7B and C). The lowest average level of RUNX2 was found in cells established from bone frozen for 30 days (Fig. 7B and C), probably reflecting increased differentiation of MSCs into osteoblasts over an extended culture period. No difference in average RUNX2 levels was observed between cells isolated from bone fragments frozen for 15 and 30 days with or without DMSO. The nuclear area was higher in cells grown from fresh bone fragments (239 ± 72 μm²), while no difference was observed between cells derived from frozen bone fragments (ranging from 145 ± 24 to 164 ± 38 μm², Fig. 7B and D). Both larger nuclei and higher RUNX2 levels probably indicate increased differentiation of MSCs to osteoblasts in cultures from fresh bones, as previously reported [44, 45]. The average RUNX2 nuclear intensity was weakly but significantly positively correlated with the nuclear area across the cell population under different conditions ($R^2 = 1.665$, $p = 1.89 \times 10^{-8}$; Fig. 7E). Taken together, these results indicate that frozen bones maintain a population of proliferating MSCs and that DMSO is not essential for preserving the osteogenic potential of these cells in the frozen bones used for autologous transplants.

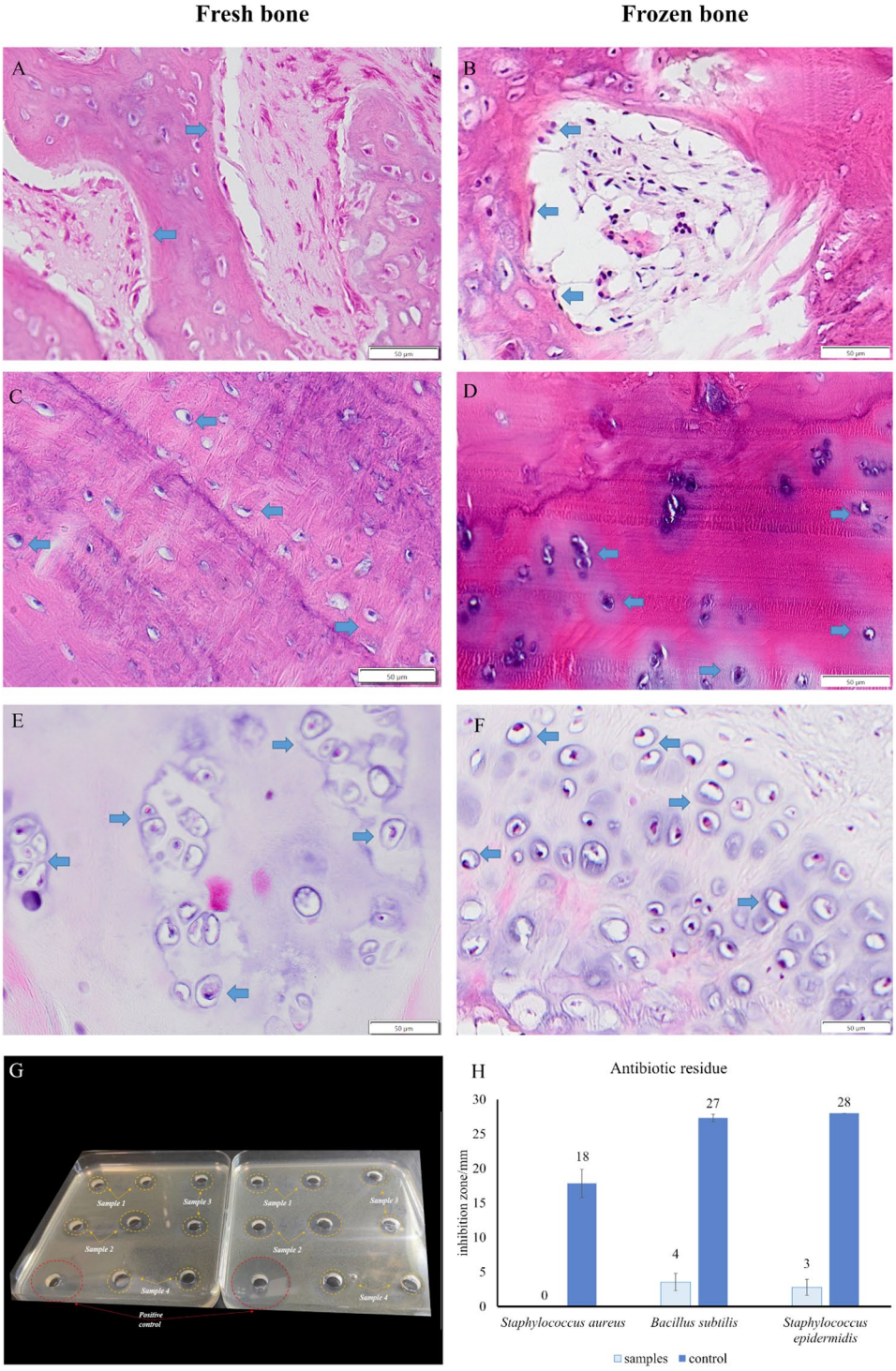

Fig. 5 Histological representation of bone fragments after contamination, decontamination, and rinsing. **A-F** Histological representation of fresh bone samples (A, C, E) and frozen bone fragments after decontamination (B, D, F). In both samples, vital osteoblasts are visible along the bone surface (A, B). Osteocytes are present in the area of the circumferential lamella within the lacunae (C, D). Visible morphology of healthy cartilage with vital chondrocytes are visible (E, F). Osteoblasts, osteocytes and chondrocytes are marked with blue arrows, respectively, scale bars, 50 µm. **G** Testing for antibiotic residues using the agar diffusion test with visible inhibition zone in control sample and minimal inhibition zone in the samples. **H** Inhibition zone for *Staphylococcus aureus*, *Bacillus subtilis* and *Staphylococcus epidermidis* from agar diffusion test

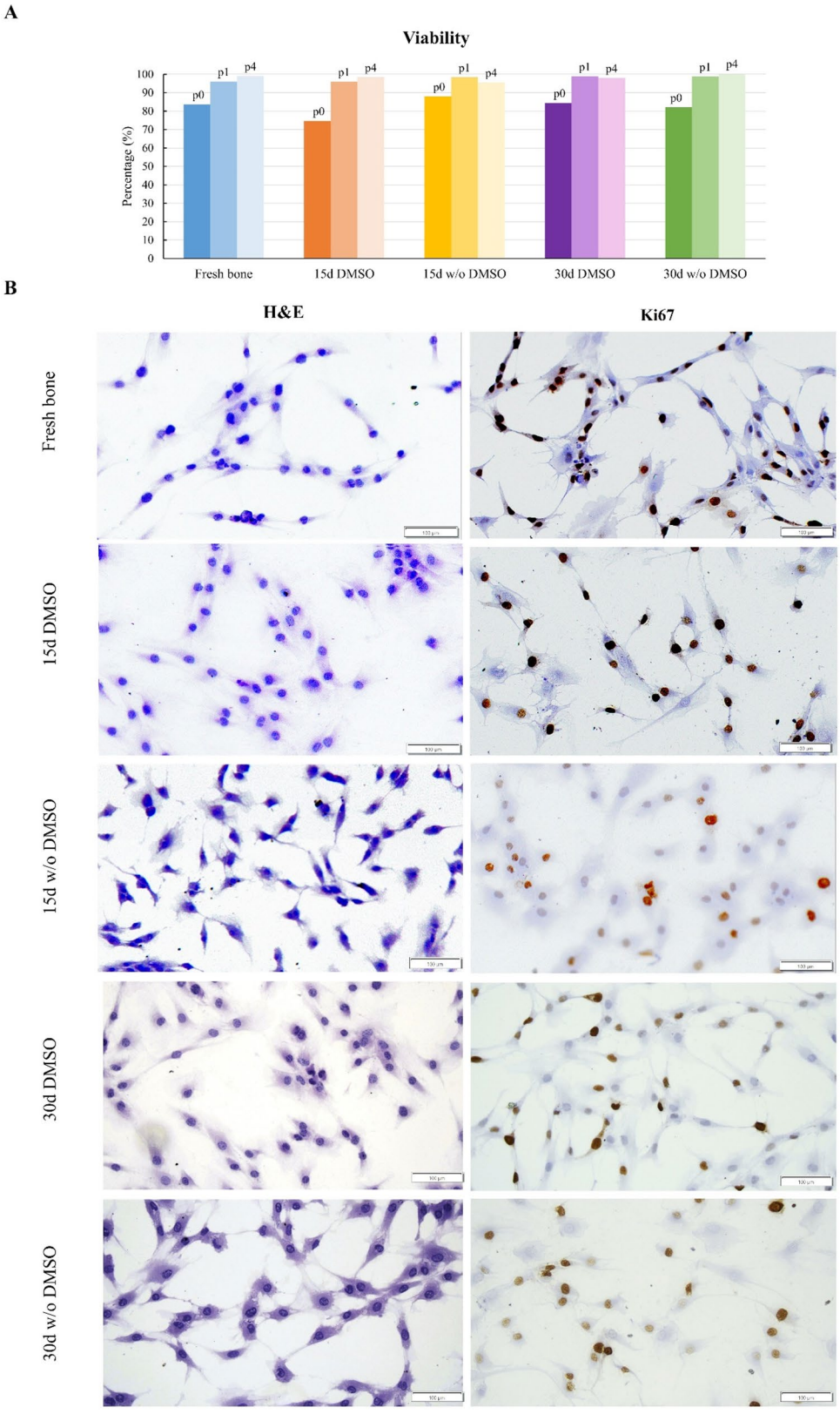

Fig. 6 (See legend on next page.)

(See figure on previous page.)

Fig. 6 Viability and proliferation of osteoblasts isolated from fresh and frozen bone fragments. **A** Viability of osteoblasts isolated from fresh bone fragments and bone fragments frozen for 15 days with and without DMSO and well as 30 days with and without DMSO in passages 0, 1 and 4. Osteoblasts in p0 were analyzed after thawing from liquid nitrogen while osteoblasts in p1 and p4 were analyzed after culturing. **B** Hematoxylin-eosin (H&E) staining of osteoblasts and IHC detection of Ki67-positive nuclei in osteoblasts (brown staining). Osteoblasts were analyzed seventh day after cultivation (p2) showing similar proliferation when isolated from both fresh and frozen bone fragments. Cells in which Ki67 is not functional, have nuclei stained purple–blue because of the presence of hematoxylin (H&E). Scale bars, 100 µm

Mitotic spindle parameters in osteoblasts in 3D To further confirm that cells isolated from frozen bone fragments are able to proliferate, we focused on describing mitotic cells found in cell cultures established from fresh and frozen bone fragments, as described above. We aimed to quantify the basic morphometry of mitotic spindles found in cultures of fresh and frozen osteoblasts, similar to our recent description of limbal stem cells grown in culture for clinical purposes [46]. Osteoblasts in culture were labeled with SiR-actin, DAPI, and α-tubulin-specific primary antibodies conjugated with a secondary antibody coupled to a green dye, and multiple fields of view of the osteoblast colonies were imaged in 3D by fluorescence confocal microscopy (see Methods). We observed mitotic cells in all phases of mitosis in cultures established from fresh and frozen bone fragments (Fig. 8A), indicating the presence of proliferating cells. The metaphase spindle length and width were on average 11.94 ± 1.75 µm and 8.02 ± 0.95 µm, respectively (Fig. 8B), which aligns with our recent measurements of mitotic limbal stem cells grown in culture [46]. Our findings indicate that frozen bone fragments contain proliferating mitotic cells that can differentiate when grown in culture.

To estimate the safety of cells grown in culture by the above-mentioned methods, we estimated the proportion of mitotic defects in proliferating cells by scoring the number of mitotic and mitotic-related defects in a fixed population of cultured osteoblasts. Defects in mitosis can lead to various cell cycle and growth abnormalities, including aneuploidy and micronuclei formation, which are hallmarks of cell transformation [47]. First, we examined the presence of nuclear abnormalities associated with aberrant mitosis, such as abnormally shaped interphase nuclei with a lobed appearance, the presence of micronuclei, and the occurrence of binucleated cells (Fig. 8C). By scoring a large number of interphase cells (n = 1452), we observed that only a small fraction (~ 2%) of the population exhibited aberrant interphase nuclei in cultured osteoblasts (Fig. 8D). To further characterize the proportion of cells with mitotic defects, we scored mitotic cells with multipolar mitotic spindles, as indicated by the tubulin signal, and anaphase/telophase cells with a chromosome bridge or lagging chromosome phenotype, identified by the DNA signal (see Methods). We found no evidence of multipolar spindles (Fig. 8E), while only ~ 5% of anaphase cells displayed a DNA signal within the spindle midzone, indicating a chromosome bridge or lagging chromosome phenotype. These findings suggest that mitotic aberrations are very rare in cell cultures grown from both fresh and frozen bones, confirming their safety.

Overall, we demonstrated that cell cultures established from frozen bone fragments robustly maintain their proliferative and differentiation capacities, irrespective of the presence of DMSO, and have low levels of mitotic defects. Moreover, the abundance of proliferating cells observed in cultures derived from both fresh and frozen bone fragments underscores their potential for further research in bone regenerative medicine.

Visualization of osteoblast cell division and morphological changes in 3D

We next monitored the time-lapse imaging of osteoblasts isolated from fresh and frozen bone fragments (n = 75) in vitro, immediately before and after cell division using 3D imaging techniques (see Methods). Analysis of the obtained data revealed that osteoblasts isolated from fresh bone fragments reach a maximum recorded height of 10.58 ± 1.85 µm before the onset of cell division, after which mitosis begins (Fig. 9A). Sixty minutes after reaching the maximum height, two cells appear, while over the next 60 min, a gradual decrease in their height is observed, accompanied by pronounced lamellipodia formation. Compared with osteoblasts isolated from fresh bone fragments, osteoblasts obtained from frozen bone fragments reach a greater maximum height just before division, averaging 12.96 ± 2.39 µm (Fig. 9B). Despite this difference, the total duration of cell division, as well as the dynamics of gradual cell height reduction and lamellipodia formation, remain unchanged between osteoblasts from fresh and frozen bone fragments. (Fig. 9). These results demonstrate that osteoblasts from frozen bone fragments not only retain the ability to undergo normal mitotic processes but also exhibit comparable dynamic behavior to those from fresh bone fragments, underscoring their adaptability and regenerative potential.

Kinetics and single-cell tracking - time-lapse imaging of osteoblasts

We next performed single cell tracking after 25-hour-long time-lapse imaging of fresh and frozen osteoblast in culture (p4) to compare movement and proliferation between fresh and frozen samples, with and without cryoprotectants (Methods). The graphs display the

movement paths of osteoblasts ($n = 187$) over a 24-hour period (Fig. 10A-C, Additional file 2). In all the samples, considerable variability in movement patterns is observed, with some cells remaining almost stationary with minimal displacement and other cells having a directed migration, usually towards a group of other cells (Fig. 10, Additional file 2). Osteoblasts tend to move in multiple different directions, although in some instances, they have similar directed migration. This is clearly visible in the direction of movement of osteoblasts isolated from fresh bone (Fig. 10A) and deep frozen for 15 days without DMSO (Fig. 10C), as multiple cells show similar migration directions. Additionally, multiple osteoblasts from these two samples also show high persistence in their movement direction while osteoblasts from the other samples (Fig. 10B, Additional file 2) show less migration, with only a few cells showing more extensive movement. Although osteoblasts mostly move at a slow, steady pace, osteoblasts isolated from fresh bone fragments (32.6 μm/h), followed by osteoblasts isolated from bone fragments deep frozen for 15 days in DMSO (27.0 μm/h), move faster than do osteoblasts in other samples (osteoblasts isolated from bone fragments deep frozen for 15 days without DMSO 25.1 μm/h, bone fragments 30 days with DMSO 24.9 μm/h and 30 days without DMSO 24.6 μm/h) (Fig. 10E). Single-cell tracking also enabled tracking of cell divisions, revealing that osteoblasts isolated from fresh bone fragments had the greatest number of divisions (14 divisions over 25 h) (Fig. 10A-C, Additional file 2). In contrast, osteoblasts from samples deep frozen for 15 days presented a reduced division rate (9 divisions), while osteoblasts from samples deep frozen for 30 days presented different numbers of divisions (Fig. 10A-C, Additional file 2). Osteoblasts isolated from fragments frozen with DMSO had 10 divisions, while the lowest number of divisions was observed in osteoblasts isolated from fragments deep frozen for 30 days without DMSO (6 divisions). These findings correlate with the population doubling times calculated for the osteoblast populations, where osteoblasts isolated from fresh bone fragments exhibited the shortest doubling time (2.24 days) (Fig. 10D).

In comparison, osteoblasts isolated from deep-frozen bone fragments with the cryoprotectant DMSO presented a population doubling time exceeding 3 days, whereas those isolated from fragments without DMSO presented a doubling time greater than 5 days (Fig. 10D). These results demonstrate that osteoblasts from fresh bone fragments exhibit superior migration, proliferation, and division rates compared to frozen samples, with cryoprotectant use partially preserving these functions. However, despite slower growth, cells from bone fragments frozen without cryoprotectants can still be expanded in vitro to similar densities.

Immunophenotypic profiling of isolated cells

To determine how the expression of MSC surface markers changes in response to bone freezing, cells isolated from fresh and frozen bone fragments with and without DMSO for 15 and 30 days were immunophenotyped at p0 and p1. The obtained fluorescence intensity results, which correlate with surface markers expression, are presented in Fig. 11.

The signal from unstained samples resulting from cell autofluorescence is also shown as a control. The cells isolated from all types of bone fragments (fresh bone and fragments frozen with and without DMSO under varying deep-freezing durations) are all negative for the hematopoietic and endothelial cell markers CD31 and CD34 and they are positive for the MSC markers CD73 and CD90, while exhibiting a slightly positive for CD146, a marker of perivascular MSCs (Fig. 11, Additional file 3). The cells in the fresh bone sample were very slightly positive for CD105. The cell population in all the samples was characterized by marker profile $CD31^{-}CD34^{-}CD73^{+}CD90^{+}$, indicating a mesenchymal phenotype. However, CD105 expression suggests that the cells have already committed to a certain differentiation lineage. Furthermore, we observed a reduction in CD73 expression in cells isolated from all frozen samples between p0 and p1. In contrast, CD90 expression increased in cells isolated from the fresh bone sample and most frozen samples, except for the sample deep frozen for 15 days with DMSO, where no increase was observed.

These findings indicate that while cells from both fresh and frozen bone fragments retain a mesenchymal phenotype, alterations in CD73 and CD90 expression key markers involved in adenosine-mediated immunosuppression and cell adhesion/stemness, respectively suggest that the functional regenerative capacity of these cells may be modified by deep-freezing.

Communication and interaction of osteoblasts in vitro (cellular cross-talk)

To determine whether osteoblasts grown in vitro after deep freezing without DMSO show signs of cell interactions and communication, we imaged the cells using light microscopy (see Methods). We observed a high generation of extracellular vesicles (EVs) and various other membrane protrusions. As shown in Fig. 12A-F, we observed retraction fibers and filopodia with EVs at their distal ends. Filopodia carrying EVs at their ends were particularly prominent and were observed in numerous cells. Furthermore, multiple cells were connected by the formation of tunneling nanotubes, as shown in Fig. 12D and E. As shown in Fig. 12E, a thickening of the nanotube suggests the possible transport of particles and organelles from unstressed to stressed cells, which might support their survival after deep freezing. Osteoblasts

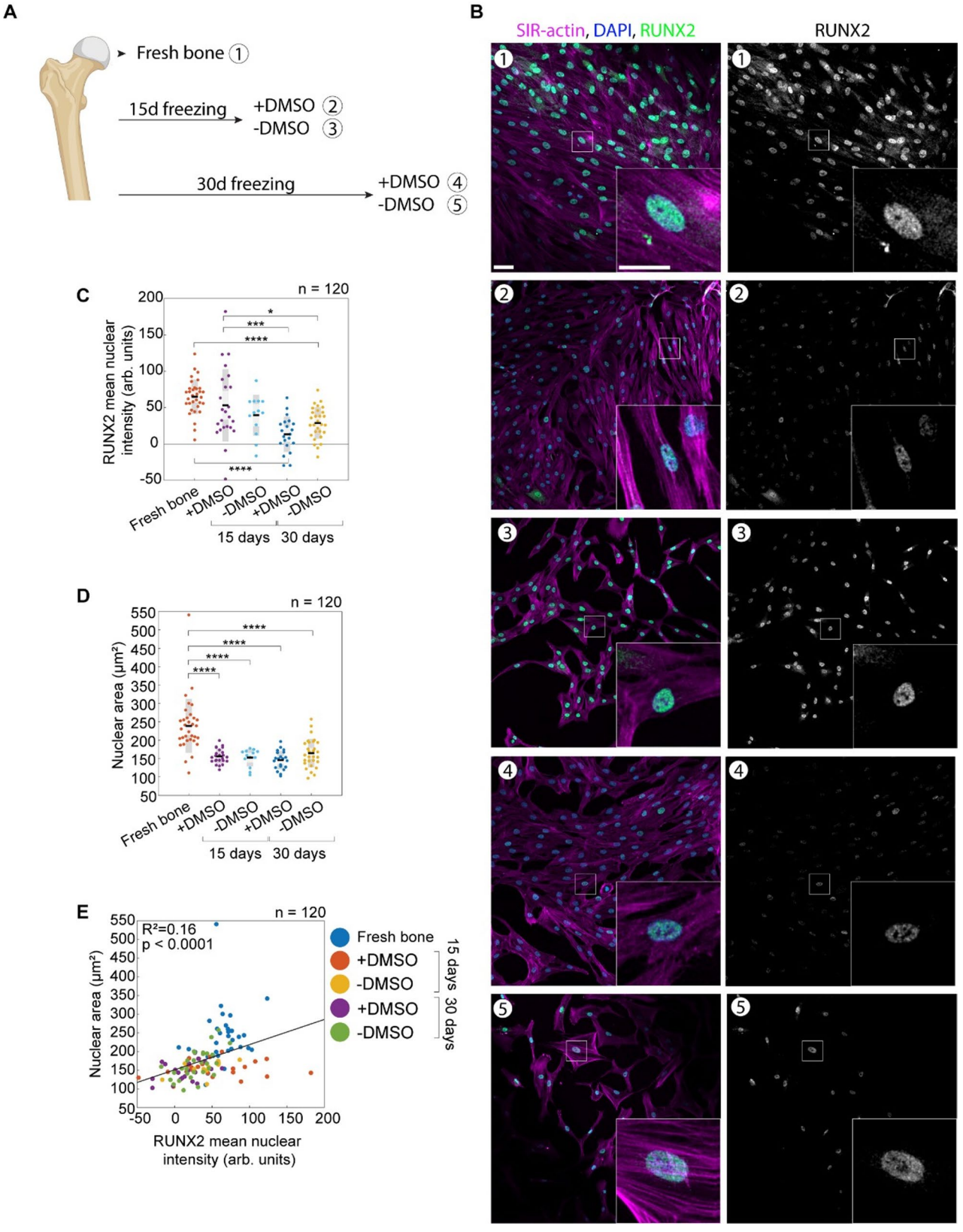

Fig. 7 (See legend on next page.)

(See figure on previous page.)

Fig. 7 Osteogenic potential of osteoblasts isolated from fresh versus frozen bone. **A** Schematic representation of the experimental protocol used to obtain cells from five conditions: fresh bone (1), bone frozen for 15 days with (2) and without DMSO (3), and bone frozen for 30 days with (4) and without DMSO (5). **B** Immunofluorescence images of cells, with the number at the top left of each image corresponding to the experimental procedure in (A). The cells were stained with SiR-Actin to label actin filaments (magenta), DAPI to label DNA (blue), and RUNX2 primary antibodies were detected using an AlexaFluor-488-conjugated secondary antibody (cyan). Merged channel images are shown on the left, while the RUNX2 channel is also displayed separately in grayscale on the right. Each image includes a zoomed-in inset of a single cell marked by a white box. Images are maximal projections of multiple z-stacks, with the signal in each channel normalized to a frozen bone sample. **C** RUNX2 mean nuclear intensity across different treatments as depicted. The black line indicates the mean, while the light and dark grey areas represent the 95% confidence interval and standard deviation, respectively. **D** Nuclear area across different treatments as depicted. **E** Scatter plot of RUNX2 mean nuclear intensity versus nuclear area, with linear regression (line) for each treatment. The right-side schematic corresponds to the experimental conditions. Statistics: Student's t test. Scale bars, 50 µm

from deep-frozen samples without DMSO exhibit robust intercellular communication, evidenced by abundant extracellular vesicles, filopodia, retraction fibers, and tunneling nanotubes that likely facilitate particle and organelle transport to support cell survival.

Induction of osteogenic differentiation and evaluation of differentiation markers

To further evaluate the molecular and phenotypic characteristics of the isolated cells, we performed osteogenic differentiation (Fig. 12J and K, see also Methods). Since fresh bone sample represent the expression status of cells without freezing, this sample (fresh bone 0 d) was used as a control for normalization of all the other samples. The *ALPL* gene expression of cells isolated from fresh bone fragments was reduced 7 days after the initiation of differentiation (Fig. 12J). Alkaline phosphatase (ALP) is a widely recognized marker of early osteoblast differentiation in vitro and plays a key role in bone formation [48, 49].

Although *ALPL* expression increased after 14 days, it did not increase above the basal expression level (fresh bone 0 d) (Fig. 12J). The *ALPL* expression of the cells isolated from a fragment deep frozen in medium containing DMSO before treatment (0 d) was lower than that of the fresh bone at the same time point (0 d). However, expression significantly increased after 7 days as well as after 14 days post-isolation (Fig. 12J). Similarly, in cells frozen for 15 days in medium without DMSO, *ALPL* expression initially decreased compared with that in fresh bone, following a similar trend observed in cells frozen for 15 days in the presence of DMSO. However, after 7 days, especially after 14 days, *ALPL* expression significantly increased (Fig. 12J).

The organic part of the bone contains more than 30 different proteins, with type I collagen (COL1) being the dominant protein (more than 90%) [50]. We explored the gene expression of *COL1A1* in fresh bone samples (Fig. 12K). The expression significantly decreased after 7 days of treatment but increased after 14 days of treatment (Fig. 12K). The pattern of cells isolated from the fragment frozen in DMSO was similar to that of the fresh bone sample. After 7 days of treatment, *COL1A1* expression significantly decreased, but it was upregulated after 14 days of treatment (Fig. 12K). In contrast, cells frozen without DMSO, which initially presented downregulation of *COL1A1* compared with that in the fresh bone sample before treatment, presented a significant increase in expression after 7 days, with an even more pronounced increase after 14 days of treatment. These results underscore the dynamic modulation of COL1A1 during osteogenic differentiation, highlighting the pivotal role of type I collagen in bone formation [50]. Notably, cells frozen without DMSO display an accelerated collagen expression profile and, upon reaching high confluence (80–90%), demonstrate a robust capacity for mineralization even without the addition of β-glycerophosphate and ascorbic acid (Fig. 12G, H) [51]. This mineralization effect was also confirmed by von Kossa staining 21 days after differentiation (Fig. 12I).

Microarray analysis

Array-CGH analysis was performed on five cultured osteoblast samples. All samples exhibited normal copy number profiles, consistent with normal female genomic patterns. Specifically, female samples showed arr(1–22,X)×2. No copy number variations of known clinical significance were detected, indicating genomic stability of the cultured osteoblasts.

Discussion

The clinical reimplementation of a large bone fragment in open femur fractures, especially when exposed to the environment due to severe trauma, presents a major challenge for tissue banks in selecting an effective decontamination method. Reimplanting a patient's own extruded bone offers significant therapeutic benefits particularly when the fragment is large, irregular, and essential for mechanical stability [21, 52, 53], . However, insufficient decontamination increases the risk of infection or nonunion ([54]. This study demonstrates the successful decontamination of a large femoral autograft and supports the use of autologous bone when feasible. Sterilization with gamma irradiation was not considered due to its potential to damage viable cells and adversely affect the biomechanical properties of the graft, which could compromise its overall quality. The present case highlights the feasibility of reimplanting a decontaminated

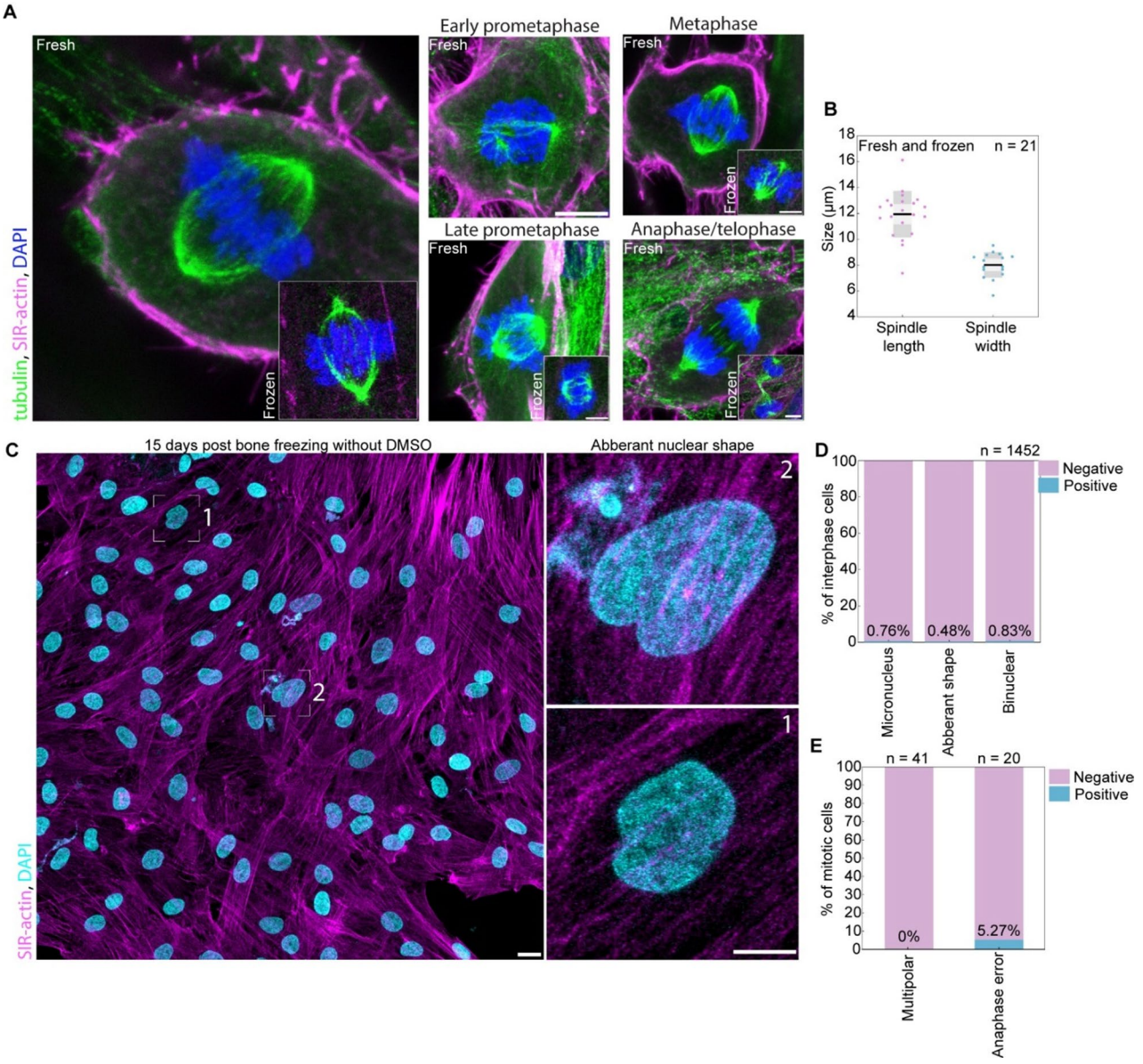

Fig. 8 Osteoblasts isolated from fresh and frozen bones do not show signs of mitotic chromosomal instability. **A** Immunofluorescence images of cells isolated from fresh and frozen bone fragments (smaller insets) in various phases of mitosis. Cells were stained with SiR-Actin to label actin filaments (magenta), DAPI to label DNA (blue), and α-tubulin primary antibodies detected with an AlexaFluor-488-conjugated secondary antibody (green) to label microtubules. Images are shown as merged channels. Scale bars, 10 µm. **B** Measurements of spindle length and width across metaphase spindles in cells isolated from fresh and frozen bones combined. **C** Immunofluorescence image of cells isolated from bones frozen for 15 days without DMSO. Cells were stained with SiR-Actin (magenta) and DAPI (cyan) to label DNA (left). Insets highlight specific cells with abnormal nuclear morphology, as indicated by the boxed region on the left (right). Scale bars, 50 µm. **D**, **E** Percentage of interphase (D) and mitotic (E) cells displaying the depicted phenotypes in cells isolated from fresh and frozen bones combined

extruded femoral segment when revascularized with a free vascularized fibular graft, achieving satisfactory biological incorporation and mechanical stability. The observed fracture union and graft hypertrophy within one year suggest that this approach can serve as a reliable limb-salvage procedure in selected cases of severe Gustilo IIIB femoral fractures. Despite postoperative challenges such as knee stiffness and instability, staged ligament reconstruction and intensive rehabilitation ultimately resulted in a favorable functional recovery and long-term structural integrity.

To study osteogenesis, we isolated osteoblasts both enzymatically and through spontaneous outgrowth from bone fragments, preserving their native characteristics. We observed that cells remained viable in bone fragments stored at – 80 °C, despite the common belief that

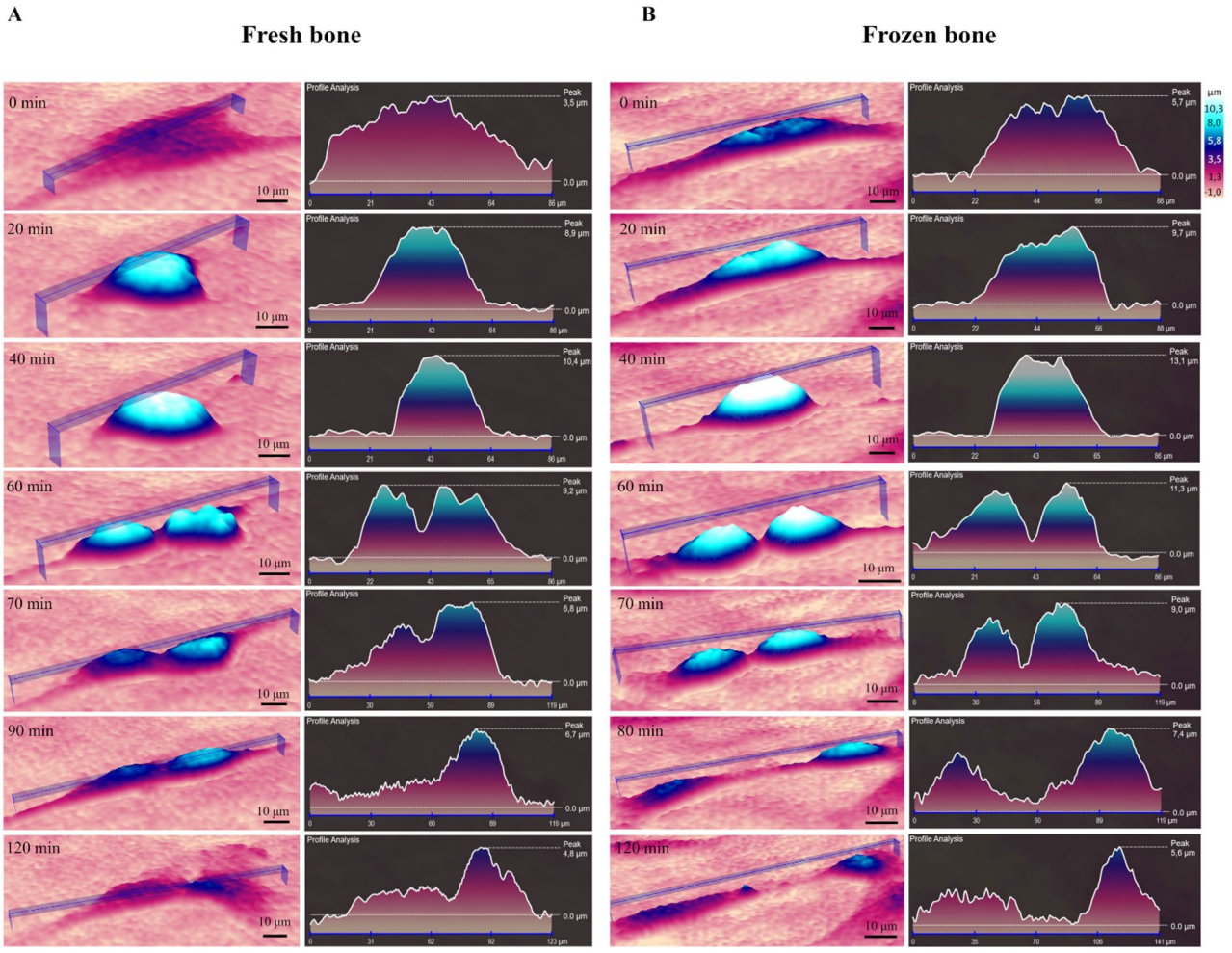

Fig. 9 Osteoblast cell division in 3D **A**. Osteoblasts isolated from fresh bone fragments initially reach a height of approximately 3.5 µm in culture. Just before division, they grow to 8.9 µm within 20 min, peaking at 10.4 µm after an additional 20 min. At this point, cell division becomes visible, with two daughter cells measuring 9.2 µm appearing after 60 min. In the following hour, the height of the cells gradually decreases, and lamellipodia begin to form. **B** Osteoblasts isolated from frozen bone fragments grow to approximately 5.7 µm in height in culture. Before division, they increase to 9.7 µm within 20 min and reach a peak of 13.1 µm after another 20 min. Cell division is clearly visible at this stage, with two cells of 11.3 µm emerging after 60 min. Over the next hour, the height of the cells gradually decreases, accompanied by the formation of lamellipodia

no living cells can survive in bone fragments frozen without DMSO. We investigated the viability of cells isolated from these bone fragments, both with and without the addition of DMSO. Cell cultures were established most rapidly from fresh bone fragments and from fragments frozen in medium containing 10% DMSO, whereas those from fragments stored without DMSO required a longer period to become established. However, once established, these cells exhibited high viability and pronounced osteogenic potential throughout subsequent passages. Cell viability, not only in bone but also in osteochondral grafts, is recognized as a key factor for successful transplantation [55, 56]. Histological analysis confirmed that viable osteoblasts, osteocytes, and chondrocytes could be recovered after freezing without cryoprotectants. In large osteochondral grafts, lower cell viability may be due to limited penetration of cryoprotectants into deeper layers, a problem observed in previous studies [57]. Their results show some chondrocyte survival occurs even without cryoprotectants. Similarly, our results show that large, frozen bone fragments retained viable osteoblasts, likely protected by their extracellular matrix. However, cryoprotectants are commonly used to increase cell survival, they can also be harmful [58, 59]. From these findings, we conclude that osteoprogenitor cells are most likely protected from cryoinjury by the bone matrix. Given that bone tissue contains very low water content, the risk of ice crystal formation and consequent cellular damage (cryoinjury) is significantly reduced.

Since cells could be cultured from frozen bone without cryoprotectants, we analyzed their morphology and molecular characteristics in cell culture and imunocytochemically. The isolated cells displayed typical osteoblastic shapes, with some exhibiting dendritic extensions

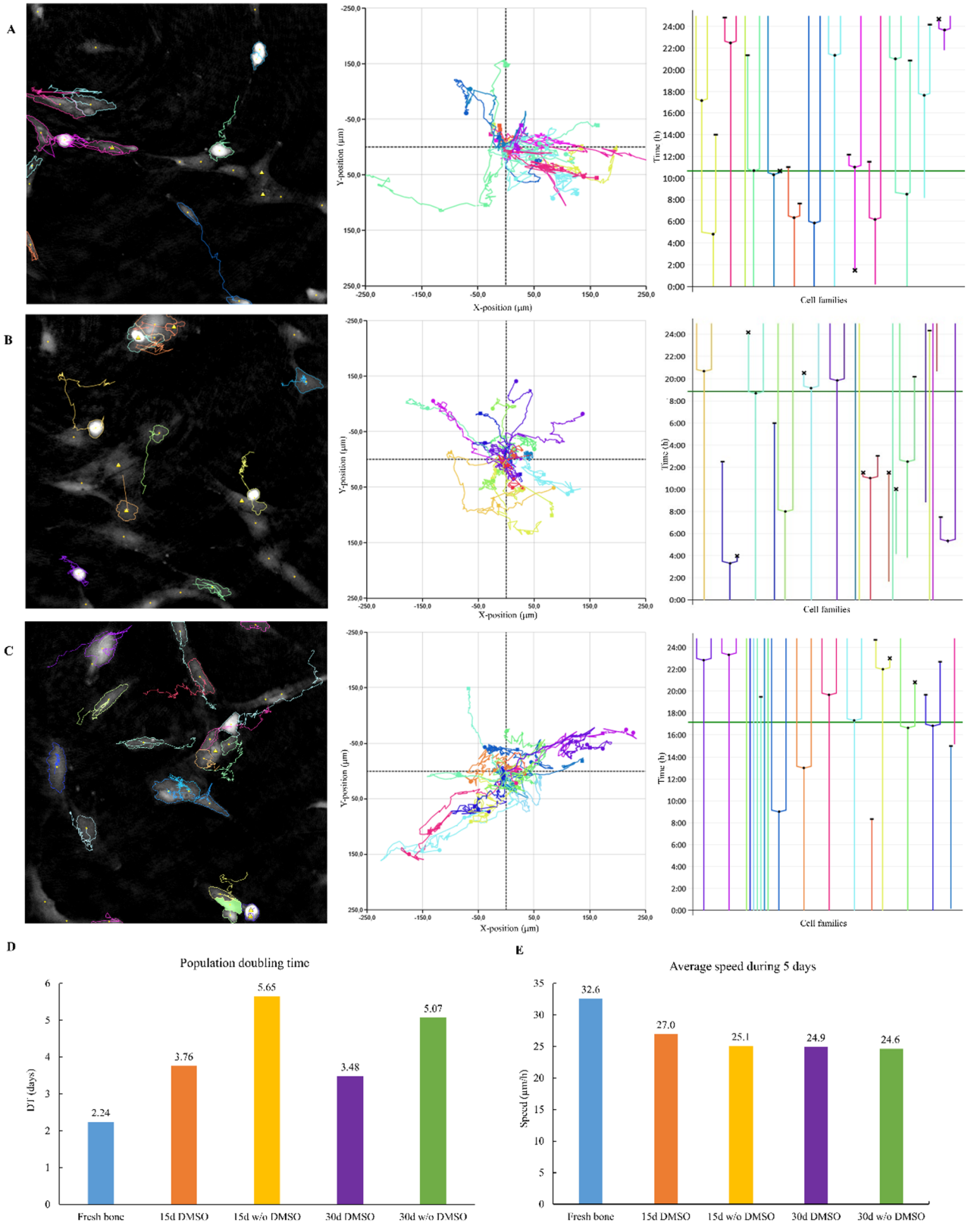

Fig. 10 (See legend on next page.)

(See figure on previous page.)

Fig. 10 Single-cell tracking and proliferation dynamics of osteoblasts. Data on cell divisions and motility were collected for osteoblasts isolated from **A** fresh bone, **B** bone fragments frozen for 15 days with DMSO, **C** bone fragments frozen for 15 days without DMSO. The tracking of individual cells is represented by the corresponding cell view at the time point indicated by the green line on the tree plot. Cell movement is depicted as lines connecting the initial and final positions of each tracked cell, with each movement trajectory color-coded accordingly. The population doubling time **D** was determined following the seeding of 30 000 osteoblasts, which were cultured for a period of 5 days to allow for proliferation. The average speed of osteoblasts **E** was calculated from the movement data recorded over a 5-day monitoring period

suggestive of osteocyte-like forms. However, as osteocytes are terminally differentiated and do not divide, the dividing cells are more likely osteoblasts, pre-osteoblasts, or osteoprogenitor cells. These retain proliferative capacity, unlike osteocytes, which are embedded in matrix and long-lived [60]. Our observations align with prior findings on osteogenic cell morphology [61, 62].

Regarding proliferative capacity, our findings suggest that osteoblasts isolated from fresh bone fragments possess the highest proliferative capacity, as evidenced by both single-cell tracking data, which monitored a small subset of cells (Fig. 10A-C, Additional file 2), and the population doubling times calculated for the entire cell population (Fig. 10D). The population doubling time of osteoblasts indicates that their proliferative capacity depends on the presence of the cryoprotectant DMSO. However, the proliferation index, calculated based on immunocytochemical analysis of Ki67 staining, showed that proliferative activity in p2 was similar in both fresh and frozen bone fragments, regardless of DMSO presence. Therefore, osteoblasts isolated from frozen bone fragments still retain the ability to proliferate through subsequent passages. Additionally, both the analysis of RUNX2 expression [63] and the morphometric assessment of mitotic spindles suggest that the proliferative capacity of osteoblasts remains comparable between cells cultured from fresh and frozen bone samples, regardless of DMSO presence. Mitotic morphology, which has been only sparsely reported in previous studies of osteoblasts derived from bone samples, was consistent across all groups and closely resembled spindle architectures observed in our recent study of limbal stem cells cultured prior to clinical application [46]. These findings indicate that osteoblasts isolated from frozen bone fragments retain the capacity to proliferate through subsequent passages.

To investigate osteoblast behavior, including migration and proliferation, over an extended period of time, we observed osteoblasts change their morphology during movement and division. Single-cell tracking revealed that all of the samples contained more static osteoblasts alongside a more migratory subset of osteoblasts. Notably, osteoblasts tend to form small colonies, and after division, daughter cells migrate toward neighboring osteoblasts. Owston compared the behavior of periosteum and bone marrow MSCs and discovered that periosteum-derived MSCs have reduced migration (20.4 μm/h for migratory cells) when compared to bone marrow MSCs (30.0 μm/h for migratory cells). The osteoblasts we analyzed over a five-day period exhibited migration speeds consistent with these findings, suggesting that osteoblasts and MSCs share similar motility characteristics (Fig. 10E). Although osteoblasts isolated from fresh bone fragments have the highest speed and deep freezing affected the migration speed of osteoblasts, it still remained within the range reported for MSCs by Owston [64]. Additionally, our goal was to observe real-time changes in osteoblasts from both fresh and frozen bone samples, including size, shape, and behavior before and after cell division. Using advanced imaging, we obtained a more detailed picture of morphological changes than traditional methods allow. Importantly, continuous monitoring of live cells under stable culture conditions eliminated the need for staining and minimized disruption, allowing for long-term observation of cell proliferation, migration, and division. To our knowledge, this single-cell tracking approach has not been previously described for osteoblasts isolated from bone fragments.

Immunophenotyping showed high mean fluorescence intensity (MFI) values for the cell surface markers CD73 and CD90 in all osteoblast samples, while slightly lower values were recorded for CD146 and CD105. Low expression levels were also observed for CD31 and CD34 (Fig. 11). These results indicate that the isolated osteoblasts are of mesenchymal origin. We observed that CD73 expression decreased from p0 to p1, with the highest intensity detected in vitro in osteoblasts isolated from bone fragments stored for 30 days without DMSO. These findings suggest that CD73 promotes osteoblast differentiation, as previously reported [65]. The marker CD90, a membrane protein associated with osteoprogenitor cells, was also highly expressed in most samples, except for those derived from fresh bone at p0. Since its expression decreases as osteoblasts mature, the elevated intensity of CD90 observed in later passages aligns with earlier studies [66]. CD146 has been described as a marker of pericytes, MSCs, and osteoblastic cells, with its expression linked to the progenitor functions of MSCs, including differentiation into osteoblasts. Our results show lower expression of CD146 compared to other mesenchymal markers in p0 and p1, consistent with previous findings that identify CD146-positive cells as a progenitor cell population [67]. CD105 was weakly expressed in all

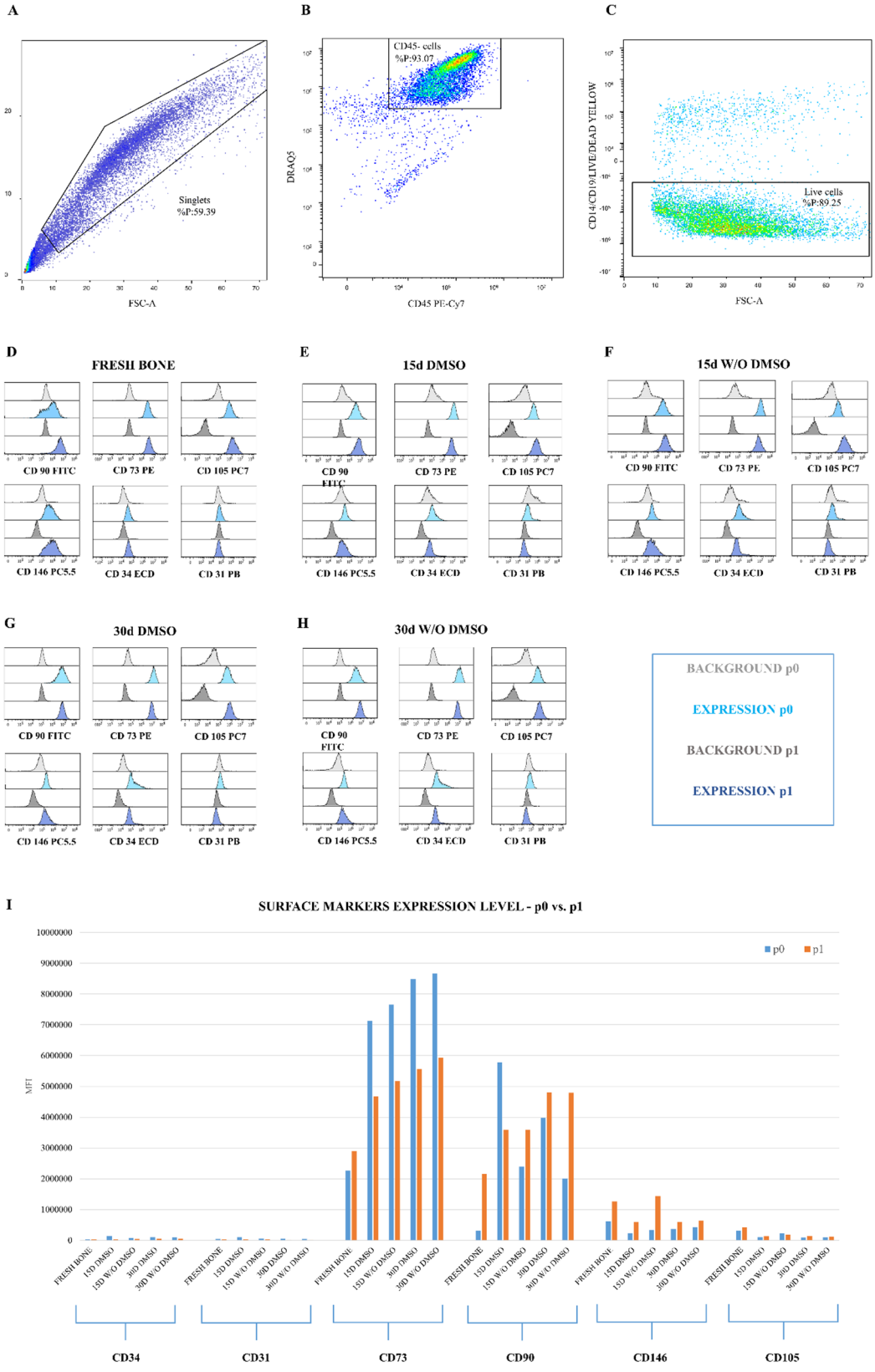

Fig. 11 (See legend on next page.)

(See figure on previous page.)

Fig. 11 Immunophenotyping of cells. The results obtained by setting the gating parameters in flow cytometry are shown. Initially, aggregates of cells (**A**) and cells expressing the CD45 marker (**B**) were excluded from the analysis. Next, only region containing CD14-CD19- viable cells was selected for further analysis (**C**). Histograms obtained after the analysis of osteoblast cells isolated from fresh bone tissue (**D**) and tissue frozen with and without DMSO over a 15-day **(E**, **F**) and 30-day period (**G**, **H**) using the DxFlex flow cytometer. The cells were analyzed using DuraClone tubes containing antibodies for the markers CD14, CD19, CD31, CD34, CD45, CD73, CD90, CD146, and CD105. In addition to the sample label, the histograms show autofluorescence and the expression of surface receptors for markers CD31, CD34, CD73, CD90, CD146, and CD105 from p0 and p1. Below each histogram, the surface marker and the fluorochrome used to label the antibodies in the DURAClone tube are indicated. (**I**) Comparison of surface level markers mean fluorescence intensity (MFI) for all the samples in p0 and p1. The results were processed using the FlowLogic software

samples, with the highest levels observed in fresh bone. We also noted low expression of CD105, indicating a significant loss of mesenchymal stem cell markers across passages, which is consistent with previously published results for MSCs [68]. Recent research suggests that different areas within skeletal tissues, such as bone marrow, articular cartilage, and periosteum, may exhibit distinct combinations of cellular markers and have multiple, functionally diverse stem cell populations [69].

In the scope of this study, we aimed to identify and characterize osteoprogenitors and osteoblasts, whose phenotype is strongly evidenced by the detection of RUNX2, a master regulator of osteogenesis ([70, 71]. While RUNX2 guides differentiation of MSCs into osteoprogenitors, the expression of *ALPL* and *COL1A1* genes reflects transitions of preosteoblasts into osteoblasts [42]. These genes serve as markers of early differentiation into the osteogenic lineage, given they have a critical role in the synthesis of bone $^{\text{matrix}}$ [70, 72]. The results regarding *ALPL* gene expression indicate that, although cryopreservation initially suppresses its early expression, cells from deep-frozen bone fragments ultimately exhibit a robust osteogenic response over time. This highlights their preserved capacity for bone formation. Consistent with these findings, the upregulation of *ALPL* as well as *COL1A1* during the differentiation period further confirmed the isolated cells are osteoprogenitors and osteoblasts as well as their osteogenic potential. Interestingly, samples frozen without cryoprotectants initially showed reduced marker expression but later exhibited a strong increase, indicating retained differentiation capacity.

We also observed intercellular communication structures, including extracellular vesicles (EVs) and membrane protrusions. EVs play a central role in bone formation by transporting minerals and enzymes required for matrix mineralization [49, 73], . In our cell cultures, matrix production occurred spontaneously once cells reached high density which is in accordance with results of Kulterer ([74] which observed black regions in cell monolayer seven days into osteogenic differentiation of bone marrow-derived MSC. Generally, osteoblasts generate mineralized bone matrix primarily through the production of specialized EVs [49,73]. These EVs are equipped with all the components necessary for formation of mineral hydroxyapatite. They possess calcium ion channels and monophosphate channels within their membranes, facilitating the import of key components necessary for hydroxyapatite synthesis. Additionally, their membranes contain the enzyme ALP, which is critical for the hydrolysis of pyrophosphate (a known inhibitor of mineralization) into monophosphate, which can subsequently be imported into the EVs for hydroxyapatite synthesis [49, 73]. While EVs typically support mineralization, their increased production, along with other structures like filopodia and nanotubes, is also associated with cellular stress responses ([75]. These authors also describe how these structures may help cells survive and communicate following freezing-induced stress (stressed cells send a "call for help" to the surrounding cells). In particular, tunneling nanotubes previously shown to aid in survival and signal exchange between stem cells ([76], may play a similar role in frozen osteoblasts. The high production of EVs and protrusions in cells frozen without cryoprotectants suggests a strong capacity for recovery and interaction despite temperature stress. EVs are essential for osteoblast communication and the regulation of bone remodeling, facilitating interactions with other osteoblasts, osteoclasts, and MSCs. They serve as key sites for initiating mineralization and carry signaling molecules that support the bone microenvironment ([77, 78]. Therefore, studying EV-mediated communication in vitro offers valuable insight into bone biology especially when comparing fresh and frozen bone-derived cells.

Direct quantification of mitotic defects in cultured osteoblasts is limited in the current literature. Here we show that osteoblasts cultured from both fresh and frozen bone samples, regardless of the presence of DMSO, exhibited minimal levels of aberrant interphase nuclear morphology, spindle geometry defects, and anaphase errors. These findings are consistent with our recent study on limbal stem cells grown in culture for clinical application [46]. As such abnormalities are considered hallmarks of tumorigenic potential in human somatic cells [79], we infer that osteoblasts derived from both fresh and cryopreserved bone samples, with or without DMSO, do not exhibit tumorigenic properties, thereby supporting their safety for potential clinical applications. We acknowledge that our conclusion regarding chromosomal stability is based on morphological assessment of mitotic and interphase integrity. Additionally, microarray analysis further substantiates the safety and chromosomal stability of all samples of cultured osteoblasts.

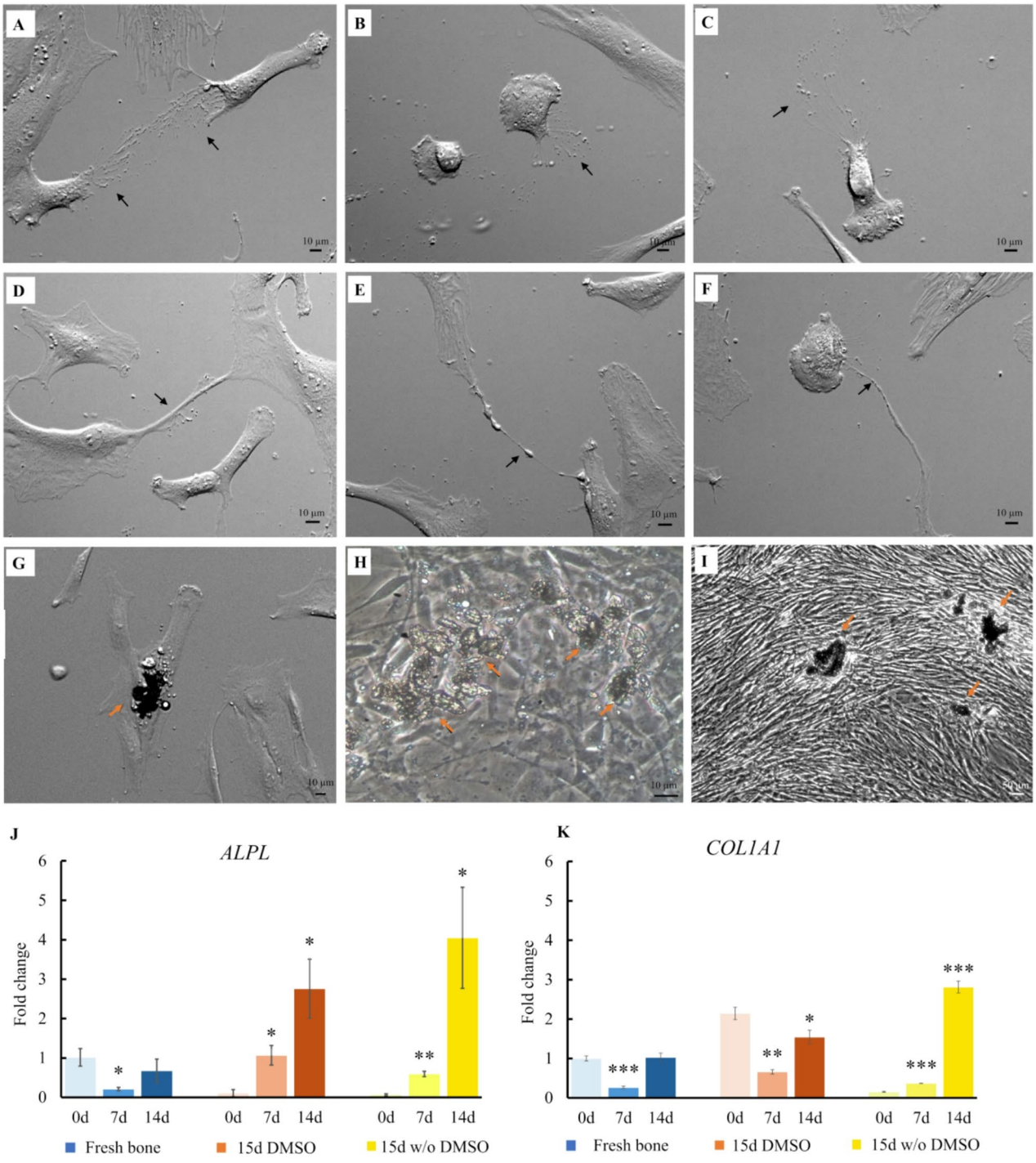

Fig. 12 Direct and indirect communication of osteoblasts and gene expression of markers of osteogenic differentiation. Osteoblasts from bone deep frozen for 15 days without DMSO exhibit indirect communication by (**A-C**) filopodia and retraction fibers, direct communication by tunneling nanotubes (stressed cells send a "call for help" to the surrounding cells) (**D**, **E**), and filopodia (**F**). Production of bone matrix in cell culture, marked with orange arrow (**G**, **H**). Detection of mineralized matrix by von Kossa in bone fragment 15d w/o DMSO, marked with orange arrow (**I**), scale bars: A-H 10 µm, I 50 µm. (**J**) Cells isolated from frozen bone fragments presented a significant increase in *ALPL* expression. (**K**) Cells isolated from bone fragments deep frozen without DMSO presented a significant increase in *COL1A1* expression. The data were normalized to the expression levels in fresh bone before differentiation (fresh bone 0d). Welch's t-tests were performed for each sample in comparison to its control (0d), $n = 3$

Although this study offers valuable insights into areas previously unexplored, several limitations must be acknowledged. First, the decontamination protocol was validated exclusively against Gram-positive microorganisms, which are the most common contaminants of musculoskeletal grafts. However, Gram-negative bacteria, though less frequently encountered, were not included in the validation, highlighting the need for future studies to evaluate the protocol's efficacy against a broader spectrum of pathogens. Another limitation concerns the biological variability inherent in donor-derived samples. While comprehensive analyses were conducted on osteoblasts isolated from both fresh and frozen bone fragments stored under various conditions (with and without cryoprotectant, at 15 and 30 days), expanding the number of donors in future research would enhance the generalizability and robustness of the findings. Furthermore, we acknowledge the limitation that, due to the small sample size, a formal power analysis could not be conducted. Nevertheless, we believe that the combination of validation of the decontamination method, histological examination, and comprehensive cytogenetic and functional cellular analyses provides sufficient evidence to support our preliminary findings.

Conclusion

The success of large autologous bone grafts depends on both effective decontamination and the preservation of viable osteoblasts after freezing. Our multidisciplinary findings demonstrate that frozen autografts, are safe and retain osteogenic potential in vitro. Osteoblasts remained metabolically active and capable of differentiation across multiple passages, supporting their role in bone regeneration and matrix maintenance. Clinically, the successful reimplantation of the large autologous bone graft confirms that appropriately decontaminated and preserved frozen bone can achieve osteointegration, representing a reliable limb-salvage strategy in cases of extensive bone loss.

Abbreviations

2D	Two-dimensional
3D	Three-dimensional
ACTB	β-actin
ALPL	Alkaline phosphatase
ATCC	American Type Culture Collection
BASE	Rinsing fluid
BASE	128 Decontamination fluid
CFU	Colony-forming units
CGH	Comparative genomic hybridization
COL1A1	Collagen type I alpha 1
CoNS	Coagulase-negative staphylococci
cPD	Cumulative population doubling
CT3P	Count-Tact® 3P® agar
DAPI	4′,6-diamidino-2-phenylindole
DMEM	Dulbecco's modified Eagle medium
DMSO	Dimethyl sulfoxide
DPBS	Dulbecco's phosphate buffer saline
DT	Doubling time
EVs	Extracellular vesicles
FA	Bottles for aerobic microbial growth
FBS	Fetal bovine serum
FN	Bottles for anaerobic microbial growth
GLA	Glutaraldehyde
H&E	Hematoxylin and eosin
HBV	Hepatitis B virus
HCV	Hepatitis C virus
HIV	Human immunodeficiency virus
IHC	Immunohistochemical
MSC	Mesenchymal stem cells
MFI	Mean fluorescence intensity
NCTC	National Collection of Type Cultures
PFA	Paraformaldehyde
qPCR	Quantitative polymerase chain reaction
ROM	Range of motion
RUNX2	Runt-related transcription factor 2
THIO-T	Thioglycollate broth with resazuin
TSA3	Trypcase soy 3P® agar
TSB-T	Trypcase soy broth

Supplementary Information

The online version contains supplementary material available at https://doi.org/10.1186/s13287-025-04839-9.

Supplementary Material 1: Inhibition zone for Staphylococcus aureus, Bacillus subtilis and Staphylococcus epidermidis from agar diffusion test, PDF; Raw data of testing for antibiotic residues using the agar diffusion test with inhibition zones in milimeters.

Supplementary Material 2: Single cell tracking, PNG; Single-cell tracking of osteoblasts (A) bone fragments frozen for 30 days with DMSO, and (B) bone fragments frozen for 30 days without DMSO. The tracking of individual cells is represented by the corresponding cell view at the time point indicated by the green line on the tree plot. Cell movement is depicted as lines connecting the initial and final positions of each tracked cell, with each movement trajectory color-coded accordingly.

Supplementary Material 3: Surface markers expression level p0 vs. p1, PDF; Quantitative summary tables of mean fluorescence intensity for all the samples in p0 and p1.

Acknowledgements

We thank Labena Croatia and Jan Cerepjuk, ing. from Czech Republic for help with APX100 digital imaging system. We are grateful to Altium Croatia who provided the HoloMonitor M4 for analysis. Sincere thanks to Kersti Alm, PhD from Phase Holographic Imaging, Sweden, for her valuable guidance regarding the HoloMonitor M4 data analysis.

Author contributions

M.Z. and M.S. planned the study and developed the methodology and experimental design. T.V. and S.M.Š. reviewed the manuscript and provided feedback. K.V., M.Đ., J.M., and I.M.T. performed data analysis related to mitotic spindle parameters in osteoblasts and evaluated osteogenic potential through immunofluorescence microscopy. M.Z., M.S., M.B.M., M.L., I.V.Z., and Z.A.S. performed the experiments. I.B. was responsible for microbiological analysis and subsequent data evaluation. S.R. and P.S. carried out ICC and IHC on osteoblasts cultivated in vitro and in bone tissue fragments. D.V., S.S., S.B., D.B., and J.P. contributed by providing bone tissue samples and clinical support for the study. D.P. and L.Z. carried out flow cytometry based immunophenotypic characterization and viability assessment of isolated osteoblasts. I.U., M.L., and Z.A.S. carried out qPCR experiments and contributed to data analysis and interpretation related to osteogenic differentiation and the expression of differentiation markers. M.L. analyzed data obtained through holographic time-lapse imaging. K.C.G. performed microarray analysis. M.Z., M.S., M.L., M.B.M., I.B., S.R., D.B., K.C.G. and K.V. wrote the manuscript. D.V. supervised the study. All authors read and approved the final manuscript.

Funding

The Tolić laboratory was funded by the European Research Council (ERC Synergy Grant, GA Number 855158), the Croatian Science Foundation (HRZZ)

through Swiss-Croatian Bilateral Projects (project IPCH-2022-10-9344), and projects co-financed by the Croatian Government and the European Union through the European Regional Development Fund—the Competitiveness and Cohesion Operational Programme: IPSted (Grant KK.01.1.04.0057) and QuantiXLie Center of Excellence (Grant KK.01.1.01.0004).

Data availability
No datasets were generated or analysed during the current study.

Declarations

Ethics approval and consent to participate
The Tissue and Cell Bank at Sestre milosrdnice University Hospital Centre, Zagreb, Croatia, holds valid authorization issued by the Ministry of Health of the Republic of Croatia for the collection, procurement, processing, testing, preservation, storage, and distribution of allogeneic bone tissue, specifically femoral heads obtained from living donors, with initial approval valid by July 17, 2014. Additional authorizations were granted on June 30, 2022, for the processing of cancellous bone tissue, and on June 20, 2022, for the handling of autologous bone. All activities were conducted in accordance with the Croatian Law on the Application of Human Tissues and Cells (NN 144/2012). The study entitled *"Harvesting, Processing, Testing, Storage, and Clinical Application of Musculoskeletal Tissue"* was reviewed by the Ethics Committee of Sestre milosrdnice University Hospital Centre at its sessions held on December 12, 2023 (Registration number: 251-29-11/3-23-05) and April 10, 2025 (Registration number: 251-29-11/3-25-11), and was approved on May 13, 2025 (Approval number: 251-29-11/3-25-17). The Committee concluded that the study is in compliance with the principles of the Declaration of Helsinki and the International Conference on Harmonisation (ICH) Guidelines for Good Clinical Practice. Written informed consent was obtained from all donors prior to sample collection.

Competing interests
The authors declare no competing interests.

Author details
[1]Department of Transfusion and Regenerative Medicine, Sestre milosrdnice University Hospital Center, Zagreb, Croatia
[2]Faculty of Biotechnology and Drug Development, University of Rijeka, Rijeka, Croatia
[3]School of Medicine, Catholic University of Croatia, Zagreb, Croatia
[4]Division of Molecular Biology, Ruđer Bošković Institute, Zagreb, Croatia
[5]Department of Traumatology, Sestre milosrdnice University Hospital Center, Zagreb, Croatia
[6]University of Applied Health Sciences, Zagreb, Croatia
[7]Department of Drug Science and Technology, University of Turin, Turin, Italy
[8]Department of Microbiology, Croatian Institute of Transfusion Medicine, Zagreb, Croatia
[9]Greyledge Europe Ltd, Zagreb, Croatia
[10]Department of Pathology and Cytology 'Ljudevit Jurak', Sestre milosrdnice University Hospital Center, Zagreb, Croatia
[11]Department of Laboratory Diagnostics, Division of Cytogenetics, University Hospital Centre Zagreb, Zagreb, Croatia
[12]School of Medicine, University of Zagreb, Zagreb, Croatia
[13]School of Medicine, University of Split, Split, Croatia
[14]Faculty of Science, Department of Biology, Zagreb, Croatia
[15]Department of anesthesiology, reanimatology and intensive care, Sestre milosrdnice University Hospital Center, Zagreb, Croatia
[16]School of Dental Medicine, University of Zagreb, Zagreb, Croatia

Received: 28 May 2025 / Accepted: 24 November 2025
Published online: 01 December 2025

References

1. Gane EM, Brakenridge CL, Smits EJ, Johnston V. The impact of musculoskeletal injuries sustained in road traffic crashes on work-related outcomes: a protocol for a systematic review. Syst Rev. 2018;7(1):1–7.
2. Centers for Disease Control and Prevention (CDC). *Transplant safety* [Internet]. Atlanta (GA): CDC; [cited 2025 Apr 5]. Available from: https://www.cdc.gov/transplant-safety/about/index.html
3. Albrektsson T, Johansson C. Osteoinduction, osteoconduction and osseointegration. Eur Spine J. 2001;10(2):96–101.
4. Khan WS, Rayan F, Dhinsa BS, Marsh D. An osteoconductive, osteoinductive, and osteogenic tissue-engineered product for trauma and orthopaedic surgery: how Far are we? Stem Cells Int. 2012;2012:236231.
5. Adamczyk A, Meulenkamp B, Wilken G, Papp S. Managing bone loss in open fractures. OTA Int. 2020;3(1):e059.
6. Willett NJ, Boninger ML, Miller LJ, Alvarez L, Aoyama T, Bedoni M, et al. Taking the next steps in regenerative rehabilitation: establishment of a new interdisciplinary field. Arch Phys Med Rehabil. 2020;101(5):917–23.
7. Park S, Rahaman KA, Kim YC, Jeon H, Han HS. Fostering tissue engineering and regenerative medicine to treat musculoskeletal disorders in bone and muscle. Bioact Mater. 2024;40:345–65.
8. Keating JF, Simpson AHRW, Robinson CM. The management of fractures with bone loss. J Bone Joint Surg Br. 2005;87(2):142–50.
9. Gustilo RB, Mendoza RM, Williams DN. Problems in the management of type III (severe) open fractures: a new classification of type III open fractures. J Trauma. 1984;24(8):742–6.
10. Gustilo RB, Merkow RL, Templeman D. The management of open fractures.fig. J Bone Joint Surg. 1990;72(2):299–304.
11. Bieber EJ, Wood MB. Bone reconstruction. Clin Plast Surg. 1986;13(4):645–55.
12. Wood MB, Cooney WP 3rd, Irons GB Jr. Skeletal reconstruction by vascularized bone transfer: indications and results. Mayo Clin Proc. 1985;60(11):729–34.
13. Shegarfi H, Reikeras O. Bone transplantation and immune response. J Orthop Surg. 2009;17(2):206–11.
14. Luk J, Stoker AM, Teixeiro E, Kuroki K, Schreiner AJ, Stannard JP, et al. Systematic review of osteochondral allograft transplant immunology: how we can further optimize outcomes. J Knee Surg. 2021;34(1):30–8.
15. Gie GA, Linder L, Ling RS, Simon JP, Slooff TJ, Timperley AJ. Impacted cancellous allografts and cement for revision total hip arthroplasty. J Bone Joint Surg Br. 1993;75(1):14–21.
16. Ling RS, Timperley AJ, Linder L. Histology of cancellous impaction grafting in the femur: a case report. J Bone Joint Surg Br. 1993;75(5):693–6.
17. Ullmark G, Linder L. Histology of the femur after cancellous impaction grafting using a Charnley prosthesis. Arch Orthop Trauma Surg. 1998;117:170–2.
18. Linder L. Cancellous impaction grafting in the human femur: histological and radiographic observations in 6 autopsy femurs and 8 biopsies. Acta Orthop Scand. 2000;71(6):543–52.
19. Shafiei Z, Bigham AS, Dehghani SN, Torabi Nezhad S. Fresh cortical autograft versus fresh cortical allograft effects on experimental bone healing in rabbits: radiological, histopathological and Biomechanical evaluation. Cell Tissue Bank. 2009;10:19–26.
20. Pipitone PS, Rehman S. Management of traumatic bone loss in the lower extremity. Orthop Clin North Am. 2014;45(4):469–82.
21. Sanders DW, Bhandari M, Guyatt G, Heels-Ansdell D, Schemitsch EH, Swiontkowski M, et al. Critical-sized defect in the tibia: is it critical? Results from the SPRINT trial. J Orthop Trauma. 2014;28(11):632–5.
22. Nauth A, Schemitsch E, Norris B, Nollin Z, Watson JT. Critical-size bone defects: is there a consensus for diagnosis and treatment? J Orthop Trauma. 2018;32(Suppl 1):S7–11.
23. Toogood P, Miclau T. Critical-sized bone defects: sequence and planning. J Orthop Trauma. 2017;31(Suppl 1):S23–6.
24. Carsenti-Etesse H, Doyon F, Desplaces N, Gagey O, Tancrede C, Pradier C, et al. Epidemiology of bacterial infection during management of open leg fractures. Eur J Clin Microbiol Infect Dis. 1999;18:315–23.
25. Aponte-Tinao LA, Ayerza MA, Muscolo DL, Farfalli GL. What are the risk factors and management options for infection after reconstruction with massive bone allografts? Clin Orthop Relat Res. 2016;474:669–73.
26. Brubaker S, Lotherington K, Zhao J, Hamilton B, Rockl G, Duong A, et al. Tissue recovery practices and bioburden: a systematic review. Cell Tissue Bank. 2016;17:561–71.
27. Paolin A, Montagner G, Petit P, Trojan D. Contamination profile in allografts retrieved from multitissue donors: longitudinal analysis. Cell Tissue Bank. 2018;19(4):809–17.
28. Tikkala S, Tirkkonen K, Ekman E, Lehtimäki K. Experience with tissue bank services in 2014 and 2020 in Turku, Finland. Transpl Proc. 2023;55(10):2345–53.
29. Pruss A, Seibold M, Benedix F, Frommelt L, von Garrel T, Gürtler L, et al. Validation of the 'Marburg bone bank system' for thermodisinfection of allogenic

femoral head transplants using selected bacteria, fungi, and spores. Biologicals. 2003;31(4):287–94.
30. Ravazzano L, Colaianni G, Tarakanova A, Xiao YB, Grano M, Libonati F. Multiscale and multidisciplinary analysis of aging processes in bone. Npj Aging. 2024;10(1):28.
31. Feng X. Chemical and biochemical basis of cell-bone matrix interaction in health and disease. Curr Chem Biol. 2009;3(2):189–96.
32. Smith CA, Richardson SM, Eagle MJ, Rooney P, Board T, Hoyland JA. The use of a novel bone allograft wash process to generate a biocompatible, mechanically stable and osteoinductive biological scaffold for use in bone tissue engineering. J Tissue Eng Regen Med. 2015;9(5):595–604.
33. Chan DYC, Mok YT, Lam PK, et al. Cryostored autologous skull bone for cranioplasty? A study on cranial bone flaps' viability and microbial contamination after deep-frozen storage at -80°C. J Clin Neurosci. 2017;42:81–3.
34. Simpson D, Kakarala G, Hampson K, Steele N, Ashton B. Viable cells survive in fresh frozen human bone allografts. Acta Orthop. 2007;78(1):26–30.
35. Deluiz D, Delcroix GJR, Fraga SRG, et al. Viable cryopreserved human bone graft exhibit superior osteogenic properties in mandibular lateral augmentation. Sci Rep. 2023;13:1422.
36. Kato Y, Boskey A, Spevak L, Dallas M, Hori M, Bonewald LF. Establishment of an osteoid preosteocyte-like cell MLO-A5 that spontaneously mineralizes in culture. J Bone Min Res. 2001;16:1622–33.
37. Zouani OF, Rami L, Lei Y, Durrieu MC. Insights into the osteoblast precursor differentiation towards mature osteoblasts induced by continuous BMP-2 signaling. Biol Open. 2013;2(9):872–81.
38. Van de Sande MAJ, Bovée JVMG, van Domselaar M, van Wijk MJ, Sanders I, Kuijper E. Successful disinfection of femoral head bone graft using high hydrostatic pressure. Cell Tissue Bank. 2018;19(3):333–40.
39. European Pharmacopoeia. Test for sterility (Ph Eur 2.6.1). Strasbourg: European Directorate for the Quality of Medicines & HealthCare (EDQM); 2009.
40. Gatto C, Giurgola L, D'Amato Tothova J. A suitable and efficient procedure for the removal of decontaminating antibiotics from tissue allografts. Cell Tissue Bank. 2013;14(1):107–15.
41. Ahmed MGT, Limmer A, Sucker C, Fares KM, Mohamed SA, Othman AH, et al. Differential regulation of CD45 expression on granulocytes, lymphocytes, and monocytes in COVID-19. J Clin Med. 2022;11(14):4219.
42. Xu JH, Li ZH, Hou YD, Fang WJ. Potential mechanisms underlying the Runx2 induced osteogenesis of bone marrow mesenchymal stem cells. Am J Transl Res. 2015;7:2527–35.
43. Martin WB, Sicard R, Namin SM, Ganey T. Methods of cryoprotectant preservation: allogeneic cellular bone grafts and potential effects. Biomed Res Int. 2019;2019:236128.
44. Ning T, Guo H, Ma M, Zha Z. BRD4 facilitates osteogenic differentiation of human bone marrow mesenchymal stem cells through WNT4/NF-κB pathway. J Orthop Surg Res. 2023;18:1–10.
45. Carroll SH, Ravid K. Differentiation of mesenchymal stem cells to osteoblasts and chondrocytes: a focus on adenosine receptors. Expert Rev Mol Med. 2013;15:e9.
46. Zekušić M, Bujić Mihica M, Skoko M, et al. New characterization and safety evaluation of human limbal stem cells used in clinical application: fidelity of mitotic process and mitotic spindle morphologies. Stem Cell Res Ther. 2023;14(1):26.
47. Santaguida S, Amon A. Short- and long-term effects of chromosome mis-segregation and aneuploidy. Nat Rev Mol Cell Biol. 2015;16:473–85.
48. Wehner C, Lettner S, Moritz A, et al. Effect of bisphosphonate treatment of titanium surfaces on alkaline phosphatase activity in osteoblasts: a systematic review and meta-analysis. BMC Oral Health. 2020;20:125.
49. Hasegawa S, Kitoh H, Ohkawara B, Mishima K, Matsushita M, Masuda A, et al. Tranilast stimulates endochondral ossification by upregulating SOX9 and RUNX2 promoters. Biochem Biophys Res Commun. 2016;470(2):356–61.
50. Mohamed AM. An overview of bone cells and their regulating factors of differentiation. Malays J Med Sci. 2008;15(1):4–12.
51. Wang Y, Huso DI, Harrington J, Kellner J, Jeong DK, Turney J, et al. Outgrowth of a transformed cell population derived from normal human BM mesenchymal stem cell culture. Cytotherapy. 2005;7(6):509–19.
52. Rathore S, Reddy IV, Ashwin Kumar AH. A novel technique for reimplanting extruded bone fragments in open fractures. Trauma Case Rep. 2016;4:5–11.
53. Hu X, Tan Q, Zhu G, Liu K. Successful reimplantation of extruded bone segment in lower limb open fractures: case report and literature review. Front Pediatr. 2024;12:1333575.
54. Afshar A. Reimplantation of a large extruded segment of bone in an open fracture. J Hand Surg Am. 2017;42(2):128–34.
55. Sherman SL, Garrity J, Bauer K, Cook J, Stannard J, Bugbee W. Fresh osteochondral allograft transplantation for the knee: current concepts. J Am Acad Orthop Surg. 2014;22(02):121–33.
56. Rosello A, Mirabet V, Fariñas O, Gelber P, Sanchís-Alfonso V. Fresh osteochondral graft. Indications, surgical technique and scientific evidence. Rev Esp Artrosc Cir Articul Engl Ed. 2021;28: 17-26.
57. Judas F, Rosa S, Teixeira L, Lopes C, Mendes AF. Chondrocyte viability in fresh and frozen large human osteochondral allografts: effect of cryoprotective agents. Transplant Proc. 2007;39(8):2531–4.
58. Best BP. Cryoprotectant toxicity: facts, issues, and questions. Rejuvenation Res. 2015;18:422–36.
59. Verheijen M, Lienhard M, Schrooders Y, Clayton O, Nudischer R, Boerno S, Timmermann B, Selevsek N, Schlapbach R, Gmuender H, Gotta S, Geraedts J, Herwig R, Kleinjans J, Caiment F. DMSO induces drastic changes in human cellular processes and epigenetic landscape in vitro. Sci Rep. 2019;9:4641.
60. Bonewald LF. The amazing osteocyte. J Bone Min Res. 2011;26(2):229–38.
61. Bernhardt A, Bacova J, Gbureck U, Gelinsky M. Influence of Cu^{2+} on osteoclast formation and activity in vitro. Int J Mol Sci. 2021;22(5):2451.
62. Franz-Odendaal TA, Hall BK, Witten PE. Buried alive: how osteoblasts become osteocytes. Dev Dyn. 2006;235(1):176–90.
63. Lian JB, Stein GS, Javed A, et al. Networks and hubs for the transcriptional control of osteoblastogenesis. Rev Endocr Metab Disord. 2006;7(1–2):1–16.
64. Owston HE, Ganguly P, Tronci G, Russell SJ, Giannoudis PV, Jones EA. Colony formation, migratory, and differentiation characteristics of multipotential stromal cells (MSCs) from clinically accessible human periosteum compared to donor-matched bone marrow MSCs. Stem Cells Int. 2019; 2019:6074245.
65. Takedachi M, Oohara H, Smith BJ, Iyama M, Kobashi M, Maeda K, et al. CD73-generated adenosine promotes osteoblast differentiation. J Cell Physiol. 2012;227(6):2622–31.
66. Dapunt U, Giese T, Stegmaier S, Moghaddam A, Hänsch GM. The osteoblast as an inflammatory cell: production of cytokines in response to bacteria and components of bacterial biofilms. BMC Musculoskelet Disord. 2016;17:243.
67. Harkness L, Zaher W, Ditzel N, Isa A, Kassem M. CD146/MCAM defines functionality of human bone marrow stromal stem cell populations. Stem Cell Res Ther. 2016;7:4.
68. Hanna H, Mir LM, Andre FM. In vitro osteoblastic differentiation of mesenchymal stem cells generates cell layers with distinct properties. Stem Cell Res Ther. 2018;9:203.
69. Cao Y, Bolam SM, Boss AL, Murray HC, Munro JT, Poulsen RC, et al. Characterization of adult human skeletal cells in different tissues reveals a $CD90^{+}$ $CD34^{+}$ periosteal stem/progenitor population. Bone. 2024;178:116926.
70. Zhu S, Chen W, Masson A, Li YP. Cell signaling and transcriptional regulation of osteoblast lineage commitment, differentiation, bone formation, and homeostasis. Cell Discov. 2024;10(1):71.
71. Komori T. Regulation of proliferation, differentiation and functions of osteoblasts by Runx2. Int J Mol Sci. 2019;20(7):1694.
72. Wischmann J, Lenze F, Thiel A, Bookbinder S, Querido W, Schmidt O, et al. Matrix mineralization controls gene expression in osteoblastic cells. Exp Cell Res. 2018;372(1):25–34.
73. Bottini M, Mebarek S, Anderson KL, Strzelecka-Kiliszek A, Bozycki L, Simão AMS, Bolean M, Ciancaglini P, Pikula JB, Pikula S, Magne D, Volkmann N, Hanein D, Millán JL, Buchet R. Matrix vesicles from chondrocytes and osteoblasts: their biogenesis, properties, functions and biomimetic models. Biochim Biophys Acta Gen Subj. 2018;1862(3):532–46.
74. Kulterer B, Friedl G, Jandrositz A, Sanchez-Cabo F, Prokesch A, Paar C, et al. Gene expression profiling of human mesenchymal stem cells derived from bone marrow during expansion and osteoblast differentiation. BMC Genomics. 2007;8:70.
75. Matejka N, Reindl J. Perspectives of cellular communication through tunneling nanotubes in cancer cells and the connection to radiation effects. Radiat Oncol. 2019;14(1):218.
76. Soundara Rajan T, Gugliandolo A, Bramanti P, Mazzon E. Tunneling nanotubes-mediated protection of mesenchymal stem cells: an update from preclinical studies. Int J Mol Sci. 2020;21(10):3481.
77. Morhayim J, Baroncelli M, van Leeuwen JP. Extracellular vesicles: specialized bone messengers. Arch Biochem Biophys. 2014;11:561.

78. Fang F, Yang J, Wang J, Li T, Wang E, Zhang D, et al. The role and applications of extracellular vesicles in osteoporosis. Bone Res. 2024;12(1):4.
79. Hanahan D, Weinberg RA. Hallmarks of cancer: the next generation. Cell. 2011;144(5):646–74.

Publisher's Note